Effect of Stratiform Heating on the Planetary-Scale Organization of Tropical Convection

QIANG DENG

Center for Prototype Climate Modeling, New York University Abu Dhabi, Abu Dhabi, UAE

BOUALEM KHOUIDER

* *Department of Mathematics and Statistics, University of Victoria, Victoria, British Columbia, Canada*

ANDREW J. MAJDA

Department of Mathematics and Center for Atmosphere and Ocean Sciences,

Courant Institute for Mathematical Sciences, New York University, New York, New York, USA

and Center for Prototype Climate Modeling, New York University Abu Dhabi, Abu Dhabi, UAE

R. S. AJAYAMOHAN

Center for Prototype Climate Modeling, New York University Abu Dhabi, Abu Dhabi, UAE

* *Corresponding author address:* Dr. Boualem Khouider, Mathematics and Statistics, University of Victoria, P.O. Box 3045, STN CSC, Victoria BC V8W 3P4, Canada.

E-mail: khouider@math.uvic.ca

ABSTRACT

It is widely recognized that stratiform heating contributes significantly to tropical rainfall and to the dynamics of tropical convective systems by inducing a front-to-rear tilt in the heating profile. Stratiform anvils forming in the wake of deep convection play a central role in the dynamics of tropical mesoscale convective systems; The wide spreading of stratiform-rain-evaporation downdrafts, originating from in the lower troposphere, strengthen the re-circulation of subsiding air in the neighborhood of the convection center and trigger cold pools and gravity currents in the boundary layer leading to further lifting, thus helping the mesoscale organization of convection. Here, aquaplanet simulations with a warm pool like surface forcing, based on a coarse-resolution GCM , of $\sim$170 km grid mesh, coupled with a stochastic multicloud parameterization, are used to demonstrate the importance of stratiform heating for the organization of convection on planetary and intraseasonal scales. When some key model parameters are set to produce higher stratiform heating fractions, the model produces low-frequency and planetary-scale MJO-like wave disturbances while lower to moderate stratiform heating fractions yield mainly synoptic-scale convectively coupled Kelvin-like waves. Furthermore, it is shown that when the effect of stratiform downdrafts is reduced in the model, the MJO-scale organization is weakened and a transition to synoptic-scale organization appears despite the use of larger stratiform heating parameters. Rooted from the stratiform instability, it is conjectured here that the strength and extent of stratiform downdrafts are key contributors to the scale selection of convective organizations perhaps with mechanisms that are in essence similar to those of mesoscale convective systems.

1. Introduction

Despite the continued progress in our understanding of precipitation and cloud processes in the tropics, their representation in coarse-resolution global climate models (GCMs) remains a challenge (Lin et al. 2006; Kim et al. 2009; Hung et al. 2013). The difficulty arises, because the underlying cumulus parameterization schemes used to represent unresolved convective process do not take into account the multi-scale character of organized tropical convection and the inherent interactions across time and spatial scales (Moncrieff and Klinker 1997; Majda 2007). At the heart of these complex interactions, tropical convection involves four main cloud types: (1) shallow cumulus clouds with tops below the temperature inversion just above the planetary boundary layer (PBL), that evolve in the subsidence regions of high convective inhibition, (2) cumulus congestus clouds with tops below the freezing level that are abundant in regions of low mid-tropospheric humidity, (3) deep convective towers that nearly reach the tropopause, which take over when the mid-troposphere is moist enough, and (4) stratiform clouds that typically develop in the upper troposphere, above the freezing level, in the wake of deep convection (Johnson et al. 1999; Lin et al. 2004; Mapes et al. 2006). We note that in contrast to stratiform clouds which expand horizontally, over a few hundred kilometres, the former three types are narrow (0.1-10 km in horizontal extent) and expand rather vertically. Their cloud base is found just above the top of the PBL, at the (first) lifting condensation level.

The occurrence of these cloud-types at a given point in time and space is largely controlled by the environmental conditions, as described above. However, due to large uncertainties and inaccuracies in the GCM state variables, a variety of cloud-type populations could in principle be present at the same time within the same GCM grid-box. Moreover, clouds have the ability to change considerably their environment either directly through exchange of latent heat associated with phase change of water and turbulent mixing (i.e. detrainment) or indirectly by modification of the radiation budget (Emanuel 1994). In this way, clouds are able to interact with each other and constitute a non-negligible source of climate variability not directly captured by the GCM mesh size or time step. In terms of latent heating, the congestus, deep, and stratiform clouds are known to affect the environment in three different ways. Cumulus congestus warm the lower troposphere and cool the upper troposphere, by radiative cooling and detrainment at cloud top, and deep convective towers warm the whole troposphere quasi-uniformly, while stratiform clouds warm the upper troposphere and cool the lower troposphere, through the evaporation of stratiform rain. In addition to the warming and cooling effects, clouds have an impact on the distribution of moisture. Pre-existing cloud-types are thus able to create conditions that are favourable or unfavourable to new cloud types. For example it is believed that congestus clouds help moisten the mid-troposphere prior to deep convection while stratiform cloud decks develop on the remains of deep convective towers. In return, the evaporative cooling induced by stratiform rain drives downdrafts that cool and dry the PBL with a twofold consequence. The cooling and drying of the PBL locally decreases the instability for moist convection (i.e. convective available potential energy, CAPE) which causes convection to cease and at the same time triggers the propagation of cold pools and gravity currents or bores which cause the deepening of the PBL in the neighbourhood of the initial cloud (Mapes 1993; Houze Jr. 1997). The PBL deepening decreases convective inhibition and allows convection to develop in the neighbourhood of an existing or recently ceased convective tower. Moreover, stratiform heating induces a front-to-rear tilted heating profile which plays a crucial role in the MJO dynamics and organized convective systems in general (Kiladis et al. 2005; Lin et al. 2004; Lappen and Schumacher 2014).

These complex processes just described are believed to be among the main mechanisms that allow convection to be "gregarious" (Mapes 1993) and lead to its organization into mesoscale cloud clusters and super-clusters (Nakazawa 1988). Nonetheless, large-scale circulation patterns associated with synoptic- and planetary-scale convective systems, such as convectively coupled equatorial waves (CCEWs) and the Madden-Julian oscillation (MJO) are believed to be favourable for convective organizations, by providing for instance large-scale convergence of moisture at low-levels. The chicken-and-egg question associated with the two-way interactions between convection and the large-scale flow is a long standing problem. However, there appears to be some sort of consensus in the tropical meteorological community that at least for the MJO initiation both bottom-up and top-down energy cascades can be encountered in nature depending on whether we are in the presence of a primary or a successive MJO event (Matthews 2008; Zhang et al. 2013). Successive MJO's seem to be triggered by the remains of preceding MJO events, in a form of circumnavigating dry Kelvin waves (Matthews et al. 1999; Ajayamohan et al. 2013) while primary MJO's are believed to be initiated in situ perhaps due to the gregarious nature of tropical clouds.

The pre-dominance of stratiform clouds in organized tropical convective systems and their importance for the latter's propagation and maintenance is widely recognized (Houze Jr. 1997; Tokay et al. 1999; Schumacher and Houze Jr. 2003; Jakob and Schumacher 2008; Sharma et al. 2009; Zhang and Hagos 2009; Tao et al. 2010). It is for instance widely recognized that the upper tropospheric outflows and implied subsidence associated with stratiform anvils play a pivotal role in the dynamics, organization, and overall morphological structure of meso-scale systems that develop in the Atlantic and Eastern Pacific ITCZ and many other parts in the globe (Dudhia and Moncrieff 1987; Parker and Johnson 2004; Khouider and Moncrieff 2015). Also several observation and modelling studies have demonstrated that stratiform clouds directly associated with deep convection and the implied tilted heating structure play a crucial role in the dynamics and propagation of the MJO and CCEWs as well as monsoon intraseasonal oscillations and low pressure systems (Lin et al. 2004; Lappen and Schumacher 2014; Choudhury and Krishnan 2011). Some important questions however remain. For example, how significantly and differently does stratiform heating and stratiform rain affect the MJO versus CCEWs? What distinguishes planetary-scale organization of tropical convection from its synoptic-scale counterpart? In this paper we use a coarse-resolution GCM with a stochastic parameterization of convection, based on the multicloud paradigm discussed above to contribute to these questions.

The multicloud model, in its deterministic version, was introduced in Khouider and Majda (2006), and further modified in Khouider and Majda (2008), as a refinement of the Majda and Shefter (2001) model for stratiform instability, which itself was inspired by Mapes (1993) and Mapes (2000). While from the linear theory point of the view, the stratiform instability yields a scale-selective-growth of moisture coupled gravity waves at synoptic scales nicely mimicking convectively coupled waves, nonlinear simulations require an additional mechanism, namely wind induced surface heat exchange (WISHE, Emanuel 1987; Neelin et al. 1987) for the maintenance and propagation of these waves (Majda et al. 2004). Also, in a warm pool setting, i.e. a horizontal distribution of the imposed sea surface temperature (SST) mimicking the Indian Ocean and Western Pacific warm pool, the wave activity occurs within the descending branch of the induced Walker cell where the surface wind is the strongest. Not only this is nonphysical but in addition, the simulation has in addition the peculiar feature of exhibiting eastward moving waves in the region of near-surface easterly winds (the eastern side) and westward waves in the region of near-surface westerlies, which is one of the main characteristics of WISHE waves.

WISHE is discarded as a viable mechanism for the MJO because it requires background easterlies to produce an MJO-like eastward moving disturbance but overall westerlies and/or very weak westerlies are observed to prevail over the Indian Ocean Western Pacific region in winter, when the MJO is most active. As demonstrated in Khouider and Majda (2006, 2008, and subsequent papers), WISHE-free waves with the right physical features are obtained when a model based on the three cloud types cumulus congestus, deep, and stratiform is used instead of only deep and stratiform. While the stratiform heating is able to destabilize the system at the right synoptic scale with the right eigen-structures of super-clusters, it is not able to sustain it. Cumulus congestus cloud decks that are observed to prevail in the front of organized convective systems of all scales are the missing link for a successful model for the two-way interactions between tropical clouds of various types and the associated large scale waves, including the MJO and CCEWs. Nonetheless, the stratiform instability remains an essential ingredient, though not the only one. As demonstrated in Majda et al. (2004), the stratiform instability is tied to the parameter μ which controls the relative contribution of stratiform heating in the downdraft closure formula. In the present study we further demonstrate that the (relative) amount of stratiform heating is the key parameter which controls the horizontal length-scale at which convection is organized in coarse-resolution GCM simulations using the stochastic multicloud model as a cumulus parameterization (Deng et al. 2015, hereafter DKM15).

The stochastic multicloud model (SMCM) was first introduced in Khouider et al. (2010) in order to take into account the unresolved variability due to interactions between various cloud types, in coarse-resolution GCMs, in the context of the multicloud model. It is used in Frenkel et al. (2012, 2013) to simulate convectively coupled gravity waves in a simplified primitive equations model. In DKM15, the SMCM was implemented in the High Order Methods Modelling Environment (HOMME) dynamical core as a cumulus parameterization for coarse-resolution GCM simulations, following Khouider et al. (2011) who previously used the deterministic MCM. Taken together, the HOMME-MCM and HOMME-SMCM models are very successful in simulating the MJO and CCEWs as well as monsoon-like intraseasonal oscillations (Khouider et al. 2011; Ajayamohan et al. 2013, 2014; DKM15). However, so far the HOMME-SMCM model is used only for the aquaplanet MJO simulations on a uniform SST background. Here we further introduce a warm pool like SST in the HOMME-SMCM model and study the sensitivity of the results to two key parameters which control the amount, i.e, the strength and temporal and spatial extent, of stratiform heating produced by the model and further investigate whether the stratiform instability mechanism is responsible for this sensitivity.

The paper is organized as follows. In Section 2, we discuss briefly the model set up and present the results of an MJO simulation in a typical parameter regime as our control simulation. Sensitivity tests to key stratiform parameters are presented in Section 3. In Section 4, we demonstrate that the effect on the planetary-scale organization due to stratiform heating can be explained in large part by the mechanism of downdrafts induced by the evaporation of stratiform rain which helps re-moisten the mid-troposphere and cool and dry the boundary layer. The latter makes cold pools that expand and strengthen with the extent and strength of the stratiform heating, and which are believed to play a major role in re-initiating new convection in the neighbouring grid cells thus leading to propagating organized convective systems, cf. the stratiform instability (Majda and Shefter 2001; Mapes 2000). A summary and conclusion is given in Section 5.

2. Model setup and control experiment

In this section we briefly review the implementation of the global atmospheric model HOMME-SMCM and highlight the key parameters which control the strength and extent of the stratiform heating, the focus of the present paper. More details on the model's framework can be found in DKM15 and the references therein. A control experiment in a typical parameter regime simulating the MJO evolution and variability within the warm pool is also presented.

a. Model setup

The SMCM-HOMME model uses the High Order Methods Modelling Environment model of the National Center for Atmospheric Research (Taylor et al. 1997; Dennis et al. 2005; Nair et al. 2009) as a dry-dynamical core coupled to the stochastic multicloud model (SMCM) of Khouider et al. (2010) as a cumulus parameterization. Apart from boundary layer and upper tropospheric damping the model is free of any other physics, expect for the cumulus heating provided by the SMCM. HOMME is a highly scalable dynamical core based on spectral elements in the horizontal and finite differences in the vertical and uses a cubed sphere geometry. In our setting, each face of the cube carries 20 integration elements of four degrees of freedom. This is roughly equivalent to a horizontal grid size of 167 km. We use 26 vertical levels and a time step of 30 seconds. The SMCM carries equations for the vertically integrated moisture and boundary layer equivalent potential temperature which are integrated in parallel with the dynamical core. The SMCM routine includes an imposed uniform cooling with a strength of roughly 1 K day^{-1} and a baroclinic vertical profile.

In the SMCM, the vertical profiles of convective heating and cooling associated with the congestus, deep, and stratiform cloud types are prescribed while the heating rates (H_c, H_d and H_s) obey the closure equations in (1).

$$\begin{aligned} H_c &= \sigma_c \frac{\alpha_c \bar{\alpha}}{H_m} \sqrt{CAPE_l^+} \\ H_d &= \sigma_d \left\{ \overline{Q} + \frac{1}{\overline{\sigma}_d \cdot \tau_{conv}} [a_1 \theta_{eb} + a_2 q - a_0(\theta_1 + \gamma_2 \theta_2)] \right\}^+ \\ H_s &= \sigma_s \alpha_s \left\{ \overline{Q} + \frac{1}{\overline{\sigma}_s \cdot \tau_{conv}} [a_1 \theta_{eb} + a_2 q - a_0(\theta_1 + \gamma_2 \theta_2)] \right\}^+ . \end{aligned} \tag{1}$$

Here q is the vertically averaged tropospheric moisture and θ_{eb} is the boundary layer equivalent potential temperature, while θ_1 and θ_2 are respectively the first and second baroclinic components associated with the vertical mode expansion (Khouider et al. 2011). The rest of the involved variables and parameters are listed in Tables 1 and 2 for the sake of streamlining. The heating profiles are based on the first and second baroclinic vertical structure basis functions so that deep convection heats the entire troposphere (up to 200 hPa) while congestus (stratiform) clouds warm (cool) the lower troposphere and cool (warm) the upper troposphere. More details can be found in Khouider et al. (2011). The combined heating profile provide the cumulus heating and cooling tendency for the temperature equation and drives the HOMME dynamical core.

The boundary layer equivalent potential temperature θ_{eb} and vertical average moisture q which appear in the closure equations in (1) satisfy,

$$\begin{aligned} \frac{\partial \theta_{eb}}{\partial t} + \mathbf{u}(x, y, p_1, t) \cdot \nabla \theta_{eb} &= \frac{1}{h} E_s - \frac{1}{h} D \\ \frac{\partial q}{\partial t} + \nabla \cdot [q(\bar{\mathbf{u}} + \mathbf{u_1} + \tilde{\alpha} \mathbf{u_2})] + \tilde{Q}_1 \nabla \cdot \mathbf{u_1} + \tilde{Q}_2 \nabla \cdot \mathbf{u_2} &= -P + \frac{D}{H}. \end{aligned} \tag{2}$$

Here E_s is the evaporation from the sea surface, and D is the downdraft mass flux:

$$\frac{1}{h}E_s = \frac{1}{\tau_e}(\theta_{eb}^* - \theta_{eb}), \quad D = \frac{m_0}{Q_{R,1}^0}[Q_{R,1}^0 + \mu(H_s - H_c)]^+(\theta_{eb} - \theta_{em}), \tag{3}$$

where θ_{eb}^* is the boundary layer saturation equivalent potential temperature and θ_{em} is the middle tropospheric equivalent potential temperature. P is the surface precipitation. In Eq. (2), $\mathbf{u}(x, y, p_1, t)$ is the horizontal velocity at the lowest model (pressure) level while $\bar{\mathbf{u}}$, $\mathbf{u}_1$, $\mathbf{u}_2$ are, respectively, the barotropic and first and second baroclinic horizontal velocity components. Here (x, y) are the longitude and latitude coordinates and ∇ is the associated horizontal gradient vector. We note that the stratiform heating directly effects the downdraft mass flux [Eq. (3)] through the parameter μ which in turn acts simultaneously on the tropospheric moisture q and the boundary layer θ_e. The latter effect drives cold pools in the boundary layer which are believed to help the initiation of new convection in the neighbouring grid cells and lead to propagating organized convective systems via the stratiform instability (Majda and Shefter 2001). The default parameters for the multicloud parameterization equations in (1), (2), and (3) are given in Table 1. They are the same as in DKM15. Unless otherwise specified, these parameter values are used throughout the present study. We note that for consistency moisture variables are expressed in temperature units.

As formulated in (1), the heating rates are proportional to the congestus, deep and stratiform cloud area fractions (σ_c, σ_d and σ_s, respectively). The cloud area fractions are simulated by a stochastic lattice model and they are the source of stochasticity, i.e. sub-grid variability, in the SMCM. Each GCM horizontal grid box is overlaid by a rectangular $n \times n$ lattice, and each lattice site is assumed to be either clear sky or occupied by a congestus, deep or stratiform cloud. The cloud area fractions are defined as the area coverage of the microscopic lattice by the sites occupied by each one of the three cloud types. A judicious coarse graining then permits to recover the exact dynamics, in the case of non-local interactions between lattice sites (Khouider et al. 2010), or approximate dynamics, in the case of nearest neighbour interactions (Khouider 2014), for the meso-scopic cloud area fraction, on the form of a three-species birth-death process at each GCM grid box.

The area-fraction birth-death process is evolved in time using Gillespie's exact algorithm (Gillespie 1975, 1977) in a straight forward fashion with very little computational overhead. Due to the extra uncertain parameters associated with local interactions, only the SMCM with non-local interactions of Khouider et al. (2010) is considered here. The implementation of the SMCM with local interactions (Khouider 2014) is left for future developments.

In the SMCM, each individual cloud site makes random transitions from one state to another according to intuitive probability rules depending on whether the environment is favourable to one cloud type or another. This leads to a Markov process with conditional transition rates. The latter are given in Table 2 for streamlining. A given rate R_{kl} goes up or goes down according to whether the environment is favourable to the associated transition or not. For instance, the transition rates from clear sky to deep convection and from congestus to deep convection both increase with both CAPE and mid-tropospheric moisteness. This mainly inhibits deep convection when the troposphere is dry to allow a more physical–progressive transition to deep convection as observed in nature.

The transition rates in Table 2 are given in terms of transition time scales denoted by τ_{kl}. They form a set of seven parameters whose values are uncertain. However some attempts to infer them from data do exist (Peters et al. 2013; De La Chevrotiere et al. 2014). To take into account the dependence of these parameters on the GCM grid resolution (in a crude way), the extra parameter τ_{grid} is introduced in FMK12. Following DKM15, here we use $\tau_{grid} = 2$. The number of lattice sites, $n \times n$ is another important parameter of the SMCM. Here we use the conservative value of $n = 40$. The sensitivity of the results to both τ_{grid} and n is documented in DKM15.

To limit the effect of the cumulus heating to the tropics, we introduce a mask in the meridional direction. It is set to one for latitudes between 30^o S and 30^o N and rapidly and smoothly decreases to zero towards the poles (Khouider et al. 2011). Moreover, a non-uniform sea surface temperature (SST) mimicking the Indian Ocean/Western pacific warm pool is imposed through the prescribed surface evaporation rate, $\frac{1}{\tau_e}(\theta^*_{eb} - \bar{\theta}_{eb})$, which is raised above its spatial mean by up to 5 K per τ_e inside the warm pool region and lowered by the same amount, outside, as illustrated in Figure 1 (see Ajayamohan et al. 2013). As shown in (1), the stratiform heating rate is controlled by two key factors, namely, the stratiform fraction α_s and the stratiform cloud area fraction σ_s. While α_s is a constant that can be adjusted directly beforehand, the area fraction σ_s is a random variable which evolves during the simulation. However, the relative strength and dynamics of the cloud area fractions are strongly modulated by the transition rates in Table 2. For instance, persistent large areas of stratiform cloud decks can be easily achieved by using large stratiform cloud decay time scale, τ_{30}, values. The same can be achieved through changes of other transition time scale combinations but here only changes in τ_{30} are considered, for the sake of simplicity.

b. Control experiment

As a first experiment, we consider the standard parameter values in Tables 1 and 2. These are essentially the same values used in DKM15 to successfully simulate the MJO on a uniform SST background except for the congestus cloud formation time scale, τ_{01}, which is increased from $\tau_{01} = 1\tau_{grid}$ to $\tau_{01} = 40\tau_{grid}$ (Table 2) and the deep cloud formation time scale, τ_{02}, which in turn is increased from $\tau_{02} = 3\tau_{grid}$ to $\tau_{02} = 4\tau_{grid}$. This allows to decrease the amount of congestus heating which otherwise leads to unrealistic results in the present warm pool setting. This due essentially to the fact that the warm pool forcing yields large CAPE values which increases the potential for congestus clouds; the transition time scales introduced here counter balances this increase in CAPE. In particular, the stratiform parameters are set to $\alpha_s = 0.50$ and $\tau_{30} = 5\tau_{grid}$.

The Hovmöller diagrams of the meridionally averaged (10^oS to 10^oN) lower level and upper level zonal winds are shown in Figure 2 followed by those of the convective heating rates, H_d, H_c, H_s and vertical average moisture, q, in Figure 3. Successive well-organized propagating convective systems are clearly seen in all of these plots, starting at the west edge of the warm pool and slowly moving to the east at roughly 5 m sec^{-1}. Moreover, the low-frequency and small-wavenumber peaks in the spectrum power plots in Figure 4 confirm the intraseasonal/planetary-scale variability which characterizes the simulation. These MJO-like events have in addition the typical quadrupole vortex and tilted vertical structures (not shown) which characterize the MJO, consistent with earlier multicloud results (Khouider et al. 2011; Ajayamohan et al. 2013; DKM15, etc).

Figure 5 depicts the time series of the cloud area fractions and heating rates averaged over a few grid points over the warm pool. As expected, the heating rates and the corresponding cloud area fractions are oscillating intensively and synchronously during the active phases of the MJO events. In particular, the area fraction time series exhibit an intermittent and yet causal variation as seen in observation, e.g., the radar data at Darwin, Australia in Peters et al. (2013).

3. Stratiform transition from CCWs to MJO regimes

Three more experiments (Table 3) are conducted to understand the response of planetary-scale organization to changes in the strength and extent of stratiform heating. As mentioned earlier, two key parameters that directly affect the stratiform heating strength and extent are α_s and τ_{30} (1). The set of all numerical experiments conducted in this study are summarized in Table 3.

In EXP2, we decrease α_s to 0.25 and keep $\tau_{30} = 5\tau_{grid}$ to separate the effect of the two parameters. The associated Hovmöller and spectrum power diagrams are shown in Figures 6, 7 and 8. From these figures we see that the variability has moved to synoptic scales and the MJO-like propagating streaks and associated low-frequency spectral power have both diminished. While a few streaks of slowly moving planetary-scale wave-like signals are still visible in the Hovmöller diagram of the 200 hPa wind, the variability of deep and stratiform heating rates and especially moisture are dominated by synoptic-scale waves that move eastward at speeds approaching 10 m sec^{-1}. While this speed is smaller than what is typically observed for convectively coupled Kelvin waves, it can be readily seen that the spectrum power is aligned linearly as it is following a dispersion-less dispersion curve of Kelvin waves with a reduced equivalent height. However, when the data is filtered following the wavenumber-frequency box shown in the spectrum power plot of deep convection in Figure 8 (a technique initially used in Wheeler and Kiladis 1999), the corresponding horizontal and vertical structures, reported in Figure 9 do not seem to resemble those of typical convectively coupled Kelvin waves. Unlike those reported in Khouider et al. (2011) for the case of a uniform SST background, the waves in Figure 9 carry a non-trivial meridional velocity converging at lower level towards the equator, within the region of active convection (corresponding roughly to the region of zonal convergence). This is consistent with the structure of Kelvin waves evolving in a meridional shear background (Ferguson et al. 2009; Han and Khouider 2010). Indeed this is unlike the MJO which instead exhibits Rossby gyres on both sides of the convection center and zonal convergence along the equator; For the MJO the meridional divergence at low level is positive, within the convection center. Nonetheless, the backward vertical tilts are still prominent as seen on the bottom panels (e, f) of Figure 9.

Next (EXP3), we keep the small value $\alpha_s = 0.25$ as in EXP2 but increase the stratiform transition time scale to $\tau_{30} = 10\tau_{grid}$. Intuitively, this will have the effect of making stratiform clouds last longer and thus expand in both time and space. In Figures 10 to 12, we show the Hovmöller and spectrum power diagrams of the meridionally averaged zonal winds and heating rates. Clearly, the planetary-scale organization of MJO-like waves are successfully recovered as in the case of EXP1.

To further demonstrate the tendency of stronger stratiform heating to yield better MJO simulation, we did another experiment with $\alpha_s = 0.75$ and $\tau_{30} = 5\tau_{grid}$ (results not shown). It resulted in similar and slightly stronger MJO-like organization than EXP1 and EXP3. However, if on the other hand we use the same large stratiform fraction $\alpha_s = 0.50$ as in EXP1 but combine it with a smaller transition time $\tau_{30} = 2\tau_{grid}$ (EXP4), similarly to EXP2 $(\alpha_s = 0.25, \tau_{30} = 5\tau_{grid})$, the planetary-scale organization of MJO-like waves is replaced by convectively coupled Kelvin waves, which as in EXP2 dominate the warm pool region (results not shown).

Two statistical measures (one being the auto-correlation function of the precipitation and column averaged moisture and the other the frequency of precipitation events) of the four experiments (EXP 1-4) are reported in Figures 13 and 14. As in DKM15, for all the experiments, the auto-correlation of the precipitation is much shorter than the moisture, which is qualitatively consistent with observational studies (e.g., Holloway and Neelin 2009, 2010). Also consistent with the results of DKM15, in the two experiments with clear MJO-like events (EXP 1 and 3), the moisture has much longer auto-correlation times. Moreover, the observed two-power-law structure of precipitation event distributions is captured in all of these four experiments consistent with the observations reported in Neelin et al. (2008) and Peters et al. (2010), consistent with the results of DKM15.

4. The stratiform organization mechanism

In this section we attempt to elucidate the physical mechanism through which the stratiform heating affects the development of planetary-scale organized MJO-like waves. The stratiform heating affects the coupled HOMME-SMCM model in two distinct fashions. One is through the differential heating and cooling of the upper and lower troposphere, which results in a tilted heating profile acting directly on the free tropospheric dynamics and the other through the moist thermodynamic variables. As already pointed out, the evaporation of stratiform rain in the lower troposphere acts as a source of mid-tropospheric re-moistening and at the same time dries and cools the boundary layer via the induced downdrafts. The latter effects are taking into account in the SMCM model via the parameter μ present in the downdraft equation [Eq. (3)]. The tilted heating is undoubtably important for successful MJO and CCWs simulation in GCMs (e.g., Khouider et al. 2011; Lappen and Schumacher 2014) but by the SMCM model design both congestus and stratiform heating contribute to the front-to-rear tilting of the MJO heating profile. Given that a strong congestus heating does not lead to a better MJO simulation, by EXP8 of this study and many other tests not reported here, it is worthwhile investigating the effect of the contribution of the stratiform heating to the downdraft field.

As demonstrated in Majda et al. (2004), through the parameter μ, the stratiform heating controls the scale-selective instability of super-clusters in terms of convectively coupled gravity waves, thus the phrase "stratiform instability". As pointed out in Majda et al. (2004), the effect of the downdraft on the boundary layer θ_e [Eq. (2)] mimics the dynamics of cold pools as they expand and spread in time and space following the stratiform heating. The stronger and more expanded the stratiform heating is, the more prominent the cold pool effect is.

Here we test this mechanism in the context of GCM simulations and see whether it can explain in part why the simulation of MJO-like planetary-scale organization versus synoptic-scale CCWs is tied to the amount of stratiform heating, as demonstrated above. To do so, we conducted a few more experiments where we keep $\alpha_s = 0.5$ and $\tau_{30} = 5\tau_{grid}$ as in EXP1 but gradually decrease the value of the parameter μ. In Figure 15, we plot the Hovmöller diagram of deep convective and congestus heating rates for the three values $\mu = 0.1$, 0.05 and 0.01. As we can see, with $\mu = 0.1$, which is equivalent to reducing the effect of stratiform heating on downdraft by a factor of roughly 2, the change in μ doesn't seem to have a big impact on the MJO simulation. In fact the MJO events seem to be more persistent and more organized than in EXP1 (Figure 3) although the heating strength seems to be a bit weaker with $\mu = 0.1$. This is indeed unlike the effect of reducing α_s by a factor of two as seen in EXP2 (Figure 7). This is in fact a clear evidence that the importance of stratiform heating, for planetary-scale organization of convection, is not limited to its contribution to the downdraft fluxes but has significant impact on the MJO and CCWs dynamics through its direct contribution to the tilting of the heating (Khouider et al. 2011; Lappen and Schumacher 2014). Nonetheless, as shown on the bottom panels (e, f) of Figure

15, when μ is reduced significantly, to $\mu = 0.01$, the planetary-scale MJO-like organization is lost but the simulation yields instead synoptic-scale eastward CCWs as in EXP2. At $\mu = 0.05$, the planetary-scale blobs of convection begin to fracture and split, though MJO-like events clearly remain visible. The progressive transition from MJO-like to synoptic-scale organization as μ decreases is confirmed by spectral power plots (not shown) although the changes are not as dramatic and as clear cut as in tuning α_s and/or τ_{03}. This suggests that MJO dynamics are very complex and cannot be explained by a single mechanism or a single variable such as column integrated moisture for example. Although, the latter is extremely important.

Another way to counter the effect of stratiform heating, both in terms of the tilted heating and its contribution to downdraft is increasing the amount of congestus heating while the stratiform parameters are kept as in EXP1. The increase of lower level heating and upper level cooling from increased congestus heating will compensate for the upper troposphere heating and lower troposphere cooling from stratiform heating, H_s. At the same time, the congestus heating rate appears in the downdraft equation [Eq. (3)], in front of H_s, with a negative sign. The former will reduce the tilt in the overall heating profile while the latter will have the effect of counterbalancing the effect of the contribution of stratiform heating to downdraft. In physical terms, the reduction of stratiform induced downdraft by congestus heating is the result of the associated compensating updrafts.

We thus repeat the simulation EXP1 but with a smaller congestus formation time scale, $\tau_{01} = 1\tau_{grid}$ (EXP8) to allow substantial growth of congestus clouds. As we can see from Figure 16, not surprisingly, this leads to CCWs type organization as in EXP2 and EXP4. This indeed confirms the importance of the two mentioned effects of stratiform heating but also the detrimental effect of over compensation by congestus heating. Nonetheless, the effect of congestus heating cannot be neglected or left aside as it is the main driver of moisture preconditioning, first by delaying deep convection and thus allowing the atmosphere to moisten through the detrainment of shallow (and congestus) clouds then by effectively driving low-level moisture convergence (Khouider and Majda 2006). The persistence of convectively coupled Rossby and Kelvin waves in this congestus dominated dry environment is consistent with the results of Khouider et al. (2011) who obtained such behaviour when the backgound moisture is weak since by the model design a dry environment promotes more congestus heating. The crucial role of congestus heating and moisture convergence have been thoroughly documented by two of the authors (e.g., Khouider and Majda 2006, 2008).

5. Summary and Conclusion

Numerical simulations using an atmospheric GCM, with an idealized water-only earth surface, with no land or topography (an aquaplanet), are presented and analyzed in terms of the ability of the model to simulate MJO-like wave disturbances. The model is based on the spectral elements HOMME dynamical core with coarse resolution using the stochastic multicloud model (SMCM) of Khouider et al. (2010) as a cumulus parameterization following DKM15. Unlike DKM15, however, here the surface forcing takes the more realistic shape of the Indian Ocean/Western Pacific warm pool. The current study focuses on the role of stratiform heating in the model's capability to reproduce organized tropical convection on multiple scales.

Many previous (modelling and observation) studies have identified stratiform heating as a major component of organized tropical convection and the MJO in particular (Moncrieff 1981; Dudhia and Moncrieff 1987; Houze Jr. 1997; Schumacher and Houze Jr. 2003; Lin et al. 2004; Parker and Johnson 2004; Mapes et al. 2006; Jakob and Schumacher 2008; Khouider et al. 2011). It is believed to be important mainly for providing the "required" tilted heating which characterizes tropical convective systems of all scales (Kiladis et al. 2009; Lin et al. 2004; Lappen and Schumacher 2014) and its ability to drive horizontal vorticity at mesoscales (Moncrieff 1981, 2010). In particular it has been identified as a source of instability for super-clusters (Mapes 2000; Majda and Shefter 2001). While many studies identified the importance of the tilted heating structure in, for example, triggering gravity waves that precondition the environment downstream to new convection (Mapes 1993; Stechmann and Majda 2009), Majda and Shefter (2001) pinpointed that the so-called "stratiform instability" is mainly a result of the acceleration of downdrafts through the evaporation of stratiform rain, which in turn drives cold pools in the boundary layer.

Here the crucial role of stratiform heating for the simulation of MJO-like convective organization in the coupled HOMME-SMCM is tested by changing a few key model parameters. In a first step, the amount of stratiform heating produced by the model was tested through two separate parameters, namely, the fraction of stratiform heating, α_s, together with the time scale that controls the decay of stratiform cloud area fraction, τ_{30}. It is found that these two parameters affect similarly the model simulations. Large values of either α_s or τ_{30} lead to planetary-scale intraseasonal MJO-like organized convection while smaller values yield synoptic-scale convectively coupled Kelvin waves. The fact that these two parameters lead to the same behaviour is not very surprising since τ_{30} strongly modulates the area fraction of stratiform heating, σ_s and that both α_s and σ_s appear as pre-factors in the stratiform heating equation (1). However, the reason why MJO simulation is so sensitive to the stratiform heating remains to be elucidated.

In order to test the role of the stratiform instability as defined in Majda and Shefter (2001) through the contribution of stratiform heating to downdrafts by the evaporation of stratiform rain mechanism, we followed up with a series of simulations using decreasing values of the parameter μ which controls the contribution of stratiform rain evaporation to downdrafts. It is found that for sufficiently small μ values, the MJO-like organization disappears and is replaced by convectively coupled Kelvin waves as in the cases with small α_s or τ_{30}. However, the amount by which μ needs to be reduced in order to shut off the MJO is not proportional to the amount by which α_s needs to be reduced in order to achieve similar results. While this clearly demonstrates the importance of stratiform induced downdrafts for MJO simulation, as it is the case for the stratiform instability, it also suggests that this is not the only mechanism that controls the scale selection of convective organization and other factors such as tilted heating may play a role. The dynamics of the MJO and organized convection in general is very complex and may not be tied to one single physical mechanism (i.e. one single model parameter) such as the tilted heating (Lappen and Schumacher 2014) or the spreading of cold pools in the boundary layer (Savarin et al. 2012; Feng et al. 2015).

This extreme sensitivity of the model simulations to stratiform heating and especially evaporation of stratiform rain raise the question about the universality of such parameters. In nature, the strength and importance of such processes is often dictated by the large scale conditions. While the amount of stratiform is clearly depending on the strength and abundance of deep convection, the dependence is not a simple linear relationship. The proportion of deep convection that is being delayed as stratiform rain is not linear nor simple. It highly depends on cloud microphysics, turbulent fluctuations in temperature and aerosol concentrations and possibly many other factors. Already, the SMCM framework takes this notion of nonlinear dependence into account through the stochastic area-fraction. However, this dependence is not strongly tied to all the physical processes that presumably control the amount of stratiform heating and especially the actual evaporation rate of stratiform rain in the lower troposphere. In state-of-the-art GCMs stratiform rain is not parameterized but directly represented through grid scale condensation. While this solves the issues of parameter tuning it lacks the observed causality associated with deep convection and the effect of sub-grid variability of the stratiform rain formation and evaporation. The authors are currently working on more realistic ways of parameterizing stratiform heating fractions using the stochastic multicloud model framework applied to comprehensive bulk mass flux column-physics cumulus parameterizations (Tiedtke 1993; Zhang and McFarlane 1995).

Acknowledgments.

The Center for Prototype Climate Modeling (CPCM) is fully funded by the Abu Dhabi Government through New York University Abu Dhabi (NYUAD) Research Institute grant.

This research was initiated and partly developed during extended visits of B.K. and A.J.M. to the CPCM at NYUAD during the years 2014 and 2015. The computations were carried out on the High Performance Computing resources at New York University Abu Dhabi.

REFERENCES

Houze Jr., R. A., 1997: Stratiform precipitation in regions of convection: A meteorological paradox? *Bull. Amer. Meteor. Soc.*, **78**, 2179–2196.

Ajayamohan, R. S., B. Khouider, and A. J. Majda, 2013: Realistic initiation and dynamics of the Madden-Julian oscillation in a coarse-resolution aquaplanet GCM. *Geophys. Res. Lett.*, **40**, 1–6, doi:10.1002/2013GL058187.

Ajayamohan, R. S., B. Khouider, and A. J. Majda, 2014: Simulation of monsoon intraseasonal oscillations in a coarse-resolution aquaplanet GCM. *Geophys. Res. Lett.*, **41**, 5662–5669, doi:10.1002/2014GL060662.

Choudhury, A. D. and R. Krishnan, 2011: Dynamical response of the south Asian monsoon trough to latent heating from stratiform and convective precipitation. *J. Atmos. Sci.*, **68**, 1347–1363.

De La Chevrotiere, M., B. Khouider, and A. Majda, 2014: Calibration of the stochastic multicloud model using bayesian inference. *SIAM J. Sci. Comput.*, **36 (3)**, B538–B560, doi:10.1137/13094267X.

Deng, Q., B. Khouider, and A. Majda, 2015: The MJO in a coarse-resolution GCM with a stochastic multicloud parameterization. *J. Atmos. Sci.*, **72**, 55–74, doi:10.1175/JAS-D-14-0120.1.

Dennis, J., A. Fournier, W. F. Spotz, A. St-Cyr, M. A. Taylor, S. J. Thomas, and H. M. Tufo, 2005: High-resolution mesh convergence properties and parallel efficiency of a spectral element atmospheric dynamical core. *International Journal of High Performance Computing Applications*, **19 (3)**, 225–235, doi:10.1177/1094342005056108.

Dudhia, J. and M. W. Moncrieff, 1987: A numerical simulation of quasi-stationary tropical convective bands. *Quart. J. Roy. Meteor. Soc.*, **113**, 929–967.

Emanuel, K. A., 1987: An air-ea interaction model of intraseasonal oscillations in the tropics. *J. Atmos. Sci.*, **44**, 2324–2340.

Emanuel, K. A., 1994: *Atmospheric convection*. Oxford University Press, 580 pp.

Feng, Z., S. Hagos, A. K. Rowe, C. D. Burleyson, M. N. Martini, and S. P. de Szoeke, 2015: Mechanisms of convective cloud organization by cold pools over tropical warm ocean during the AMIE/DYNAMO field campaign. *J. Adv. Model. Earth Syst.*, **07**, 1–25, doi:10.1002/2014MS000384.

Ferguson, J., B. Khouider, and M. Namazi, 2009: Two-way interactions between equatorially trapped waves and the barotropic flow. *Chin. Ann. Math*, **30B**, 539–568.

Frenkel, Y., A. J. Majda, and B. Khouider, 2012: Using the stochastic multicloud model to improve tropical convective parameterization: A paradigm example. *J. Atmos. Sci.*, **69**, 1080–1105, doi:10.1175/JAS-D-11-0148.1.

Frenkel, Y., A. J. Majda, and B. Khouider, 2013: Stochastic and deterministic multicloud parameterizations for tropical convection. *Clim. Dyn.*, **41**, 1527–1551, doi:10.1007/s00382-013-1678-z.

Gillespie, D. T., 1975: An exact method for numerically simulating the stochastic coalescence process in a cloud. *J. Atmos. Sci.*, **32**, 1977–1989.

Gillespie, D. T., 1977: Exact stochastic simulation of coupled chemical reactions. *J. Phys. Chem.*, **81**, 2340–2361.

Han, Y. and B. Khouider, 2010: Convectively coupled waves in a sheared environment. *J. Atmos. Sci.*, **67**, 2913–2942.

Holloway, C. E. and J. D. Neelin, 2009: Moisture vertical structure, column water vapor, and tropical deep convection. *J. Atmos. Sci.*, **66**, 1665–1683.

Holloway, C. E. and J. D. Neelin, 2010: Temporal relations of column water vapor and tropical precipitation. *J. Atmos. Sci.*, **67**, 1091–1105.

Hung, M.-P., J.-L. Lin, W. Wang, D. Kim, T. Shinoda, and S. J. Weaver, 2013: MJO and convectively coupled equatorial waves simulated by CMIP5 climate models. *J. Climate*, **26**, 6185–6214.

Jakob, C. and C. Schumacher, 2008: Precipitation and latent heating characteristics of the major tropical western Pacific cloud regimes. *Journal of Climate*, **21**, 4348–4364.

Johnson, R. H., T. M. Rickenbach, S. A. Rutledge, P. E. Ciesielski, and W. H. Schubert, 1999: Trimodal characteristics of tropical convection. *J. Climate*, **12**, 2397–2418.

Khouider, B., 2014: A coarse grained stochastic multi-type particle interacting model for tropical convection: nearest neighbour interactions. *Comm. Math. Sci.*, **12 (8)**, 1379–1407, doi:10.4310/CMS.2014.v12.n8.a1.

Khouider, B., J. Biello, and A. J. Majda, 2010: A stochastic multicloud model for tropical convection. *Comm. Math. Sci.*, **8**, 187–216.

Khouider, B. and A. J. Majda, 2006: Model multi-cloud parameterizations for convectively coupled waves: Detailed nonlinear wave evolution. *Dyn. Atmos. Oceans*, **42**, 59–80.

Khouider, B. and A. J. Majda, 2008: Multicloud models for organized tropical convection: Enhanced congestus heating. *J. Atmos. Sci.*, **65**, 897–914.

Khouider, B. and M. Moncrieff, 2015: Organized convection parameterization for the ITCZ. *J. Atmos. Sci.*, in press, doi:10.1175/JAS-D-15-0006.1.

Khouider, B., A. St-Cyr, A. J. Majda, and J. Tribbia, 2011: The MJO and convectively coupled waves in a coarse-resolution GCM with a simple multicloud parametrization. *J. Atmos. Sci.*, **68**, 240–264, doi:10.1175/2010JAS3443.1.

Kiladis, G. N., K. Straub, and P. Haertel, 2005: Zonal and vertical structure of the Madden-Julian oscillation. *J. Atmos. Sci.*, **62**, 2790–2809.

Kiladis, G. N., M. C. Wheeler, P. T. Haertel, K. H. Straub, and P. E. Roundy, 2009: Convectively coupled equatorial waves. *Rev. Geophys.*, **47**, RG2003, doi:10.1029/2008RG000266.

Kim, D., et al., 2009: Application of MJO simulation diagnostics to climate models. *J. Climate*, **22**, 6413–6436.

Lappen, C.-L. and C. Schumacher, 2014: The role of tilted heating in the evolution of the MJO. *J. Geophys. Res. Atmos.*, **119**, 2966–2989.

Lin, J.-L., B. Mapes, M. Zhang, and M. Newman, 2004: Stratiform precipitation, vertical heating profiles, and the Madden-Julian oscillation. *J. Atmos. Sci.*, **61**, 296–309.

Lin, J.-L., et al., 2006: Tropical intraseasonal variability in 14 IPCC AR4 climate models. Part I: Convective signals. *J. Climate*, **19**, 2665–2690.

Majda, A. J., 2007: New multiscale models and self-similarity in tropical convection. *J. Atmos. Sci.*, **64**, 1393–1404.

Majda, A. J., B. Khouider, G. N. Kiladis, K. H. Straub, and M. G. Shefter, 2004: A model for convectively coupled tropical waves: Nonlinearity, rotation, and comparison with observations. *J. Atmos. Sci.*, **61**, 2188–2205.

Majda, A. J. and M. Shefter, 2001: Models for stratiform instability and convectively coupled waves. *J. Atmos. Sci.*, **58**, 1567–1584.

Mapes, B., S. Tulich, J. Lin, and P. Zuidema, 2006: The mesoscale convection life cycle: Building block or prototype for large-scale tropical waves? *Dyn. Atmos. Oceans*, **42**, 3–29, doi:10.1016/j.dynatmoce.2006.03.003.

Mapes, B. E., 1993: Gregarious tropical convection. *J. Atmos. Sci.*, **50**, 2026–2037.

Mapes, B. E., 2000: Convective inhibition, subgrid-scale triggering energy, and stratiform instability in a toy tropical wave model. *J. Atmos. Sci.*, **57**, 1515–1535.

Matthews, A., J. M. Slingo, B. J. Hoskins, and P. M. Inness, 1999: Fast and slow kelvin waves in the Madden-Julian oscillation of a GCM. *Q.J.R. Meteorl. Soc.*, **125**, 1473–1498.

Matthews, A. J., 2008: Primary and successive events in the Madden-Julian oscillation. *Quart. J. Roy. Meteor. Soc.*, **134**, 439–453.

Moncrieff, M. W., 1981: A theory of organized steady convection and its transport properties. *Quart. J. Roy. Meteor. Soc.*, **107**, 29–50.

Moncrieff, M. W., 2010: The multiscale organization of moist convection and the intersection of weather and climate. why does climate vary? *Geophys. Monogr., No. 189, Amer. Geophys. Union*, 3–26, doi:doi:10.1029/2008GM000838.

Moncrieff, M. W. and E. Klinker, 1997: Organized convective systems in the tropical western Pacific as a process in general circulation models: A TOGA COARE case-study. *Quart. J. Roy. Meteor. Soc.*, **123**, 805–827.

Nair, R. D., H.-W. Choi, and H. Tufo, 2009: Computational aspects of a scalable high-order discontinuous Galerkin atmospheric dynamical core. *Computers & Fluids*, **38 (2)**, 309–319, doi:10.1016/j.compfluid.2008.04.006.

Nakazawa, T., 1988: Tropical superclusters within intraseasonal variations over the western Pacific. *J. Meteor. Soc. Japan*, **66**, 777–786.

Neelin, J. D., I. M. Held, and K. H. Cook, 1987: Evaporation-wind feedback and low-frequency variability in the tropical atmosphere. *J. Atmos. Sci.*, **44**, 2341–2348.

Neelin, J. D., O. Peters, J. W. B. Lin, K. Hales, and C. E. H. CE, 2008: Rethinking convective quasi-equilibrium: observational constraints for stochastic convective schemes in climate models. *Phil. Trans. R. Soc. A*, **366**, 2579–2602.

Parker, M. D. and R. H. Johnson, 2004: Structures and dynamics of quasi-2d mesoscale convective systems. *J. Atmos. Sci.*, **61**, 545–567.

Peters, K., C. Jakob, L. Davies, B. Khouider, and A. Majda, 2013: Stochastic behavior of tropical convection in observations and a multicloud model. *J. Atmos. Sci.*, **70**, 3556–3575, doi:10.1175/JAS-D-13-031.1.

Peters, O., A. Deluca, A. Corral, J. D. Neelin, and C. E. Holloway, 2010: Universality of rain event size distributions. *J. Stat. Mech. Theory Exp.*, P11030, doi:10.1088/1742-5468/2010/11/P11030.

Savarin, A., S. S. Chen, B. W. Kerns, C. Lee, and D. P. Jorgensen, 2012: Convective Cold Pool Structure and Boundary Layer Recovery in DYNAMO. *AGU Fall Meeting Abstracts*, A211.

Schumacher, C. and R. A. Houze Jr., 2003: Stratiform rain in the tropics as seen by the TRMM precipitation radar. *Journal of Climate*, **16**.

Sharma, S., M. Konwar, D. K. Sarma, M. C. R. Kalapureddy, and A. R. Jain, 2009: Characteristics of rain integral parameters during tropical convective, transition, and stratiform rain at Gadanki and its application in rain retrieval. *Journal of Applied Meteorology and Climatology*, **48**, 1245–1266.

Stechmann, S. N. and A. J. Majda, 2009: Gravity waves in shear and implications for organized convection. *J. Atmos. Sci*, **66**, 2579–2599.

Tao, W.-K., S. Lang, X. Zeng, S. Shige, and Y. Takayabu, 2010: Relating convective and stratiform rain to latent heating. *Journal of Climate*, **23**, 1874–1893.

Taylor, M., J. Tribbia, and M. Iskandarani, 1997: The spectral element method for the shallow water equations on the sphere. *Journal of Computational Physics*, **130 (1)**, 92–108, doi:10.1006/jcph.1996.5554.

Tiedtke, M., 1993: Representation of clouds in large-scale models. *Mon. Weather Rev.*, **121 (11)**, 3040–3061.

Tokay, A., D. A. Short, C. R. Williams, W. L. Ecklund, and K. S. Gage, 1999: Tropical rainfall associated with convective and stratiform clouds: Intercomparison of disdrometer and profiler measurements. *Journal of Applied Meteorology*, **38**.

Wheeler, M. and G. N. Kiladis, 1999: Convectively coupled equatorial waves: Analysis of clouds and temperature in the wavenumber-frequency domain. *J. Atmos. Sci.*, **56**, 374–399.

Zhang, C., J. Gottschalck, E. Maloney, M. Moncrieff, F.Vitart, D. Waliser, B. Wang, and M. Wheeler, 2013: Cracking the MJO nut. *Geophys. Res. Lttr.*, doi:DOI:10.1002/grl.50244.

Zhang, C. and S. M. Hagos, 2009: Bi-modal structure and variability of large-scale diabatic heating in the tropics. *Journal of the Atmospheric Sciences*, **66**, 3621–3640.

Zhang, G. J. and N. A. McFarlane, 1995: Sensitivity of climate simulations to the parameterization of cumulus convection in the Canadian Climate Center general circulation model. *Atmos. Ocean*, **33 (3)**, 407–446.

List of Tables

TABLE 1. List of the default multicloud parameters for SMCM-HOMME. $\tilde{Q}_j$ in parentheses corresponding to a normalization with the L_2 norm of the basis function ϕ_j that enter in the projections of the horizontal velocity field.

Parameter	Value	Description
$\tilde{Q}_1$ $\tilde{Q}_2$	38.47 K 38.35 K	First baroclinic projection of the background moisture gradient in Eq.(2) Second baroclinic projection of the background moisture gradient in Eq.(2)
$Q^0_{R,1}$ $\bar{\theta}_{eb} - \bar{\theta}_{em}$ $\bar{\theta}^*_{eb} - \bar{\theta}_{eb}$	1K/day 11.00K 10.00K	First baroclinic radiative cooling rate Discrepancy between θ_{eb} and θ_{em} at RCE in Eq.(3) Discrepancy between saturation and actual θ_{eb} at RCE in Eq.(3)
a_1/a_2	0.1 / 0.9	Relative contribution of θ_{eb}/q to deep convection in (1)
a_0	0.5	Dry convective buoyancy frequency in deep and congestus heating in (1)
γ_2/γ_2'	0.25 / 0.6	Relative contribution of θ_2 to deep/congestus heating in (1) and to $CAPE/CAPE_l$ in Table 2
μ	0.2	Relative contribution of stratiform and congestus to downdrafts in Eq.(3)
α_c/α_s	0.25 / 0.5	Congestus/stratiform adjustment coefficient in (1)
τ_c/τ_s	1 hr / 3 hrs	Congestus/stratiform adjustment time scale in (1)
τ_{conv}	2h	Convective time scale in (1)
h H	500 m 16 km	Prescribed boundary layer height Average height of the tropical tropsphere
$m_0 = \overline{P} \cdot Q^0_{R,1}/[Q^0_{R,1} + \mu(\overline{H}_s - \overline{H}_c)] \cdot 1/(\bar{\theta}_{eb} - \bar{\theta}_{em}) \cdot H$	0.00734 m sec^{-1} (in EXP1)	Scale of downdraft mass flux, value set by RCE solution
$\tau_e = (\bar{\theta}^*_{eb} - \bar{\theta}_{eb}) \cdot h/(\overline{P} \cdot H)$	14.8 hrs (in EXP1)	Evaporation time scale, value set by RCE solution
$\tilde{\alpha}$	0.1	Coefficient of second barcolinic velocity component in moisture equation
R	320 J/kg K^{-1}	CAPE constant in Table 2
γ	1.7	Contribution of θ_1 to CAPE anomalies in Table 2
T_0	30 K	Scaling factor of dryness in Table 2
CAPE_0	400 J/kg	Scaling factor of CAPE in Table 2
$n \times n$	1600	Number of lattice sites within each CGM grid box

Table 2. Transition rates and time scales in the stochastic parametrization.

Transition	Transition Rate	Time scale (h)
Formation of congestus	$R_{01} = \frac{1}{\tau_{01}}\Gamma(C_l)\Gamma(D)$	$\tau_{01} = 40\tau_{grid}$
Decay of congestus	$R_{10} = \frac{1}{\tau_{10}}\Gamma(D)$	$\tau_{10} = 1\tau_{grid}$
Conversion of congestus to deep	$R_{12} = \frac{1}{\tau_{12}}\Gamma(C)[1-\Gamma(D)]$	$\tau_{12} = 1\tau_{grid}$
Formation of deep	$R_{02} = \frac{1}{\tau_{02}}\Gamma(C)[1-\Gamma(D)]$	$\tau_{02} = 4\tau_{grid}$
Conversion of deep to stratiform	$R_{23} = \frac{1}{\tau_{23}}$	$\tau_{23} = 3\tau_{grid}$
Decay of deep	$R_{20} = \frac{1}{\tau_{20}}[1-\Gamma(C)]$	$\tau_{20} = 3\tau_{grid}$
Decay of stratiform	$R_{30} = \frac{1}{\tau_{30}}$	$\tau_{30} = 2$ or 5 or $10\tau_{grid}$

$$\Gamma(x) = \begin{cases} 1-\exp(-x), & \text{if } x > 0; \\ 0, & \text{otherwise.} \end{cases} \qquad D = (\theta_{eb} - \theta_{em})/T_0$$

$$CAPE_l = \overline{CAPE} + R[\theta_{eb} - \gamma(\theta_1 + \gamma_2'\theta_2)], \quad C_l = CAPE_l/CAPE_0$$

$$CAPE = \overline{CAPE} + R[\theta_{eb} - \gamma(\theta_1 + \gamma_2\theta_2)], \quad C = CAPE/CAPE_0$$

TABLE 3. List of the experiments with different stratiform heating strength.

Experiment	Stratiform heating coefficient (α_s)	Stratiform decay time scale (τ_{30})	Other changes
EXP1	0.50	$5\tau_{grid}$	
EXP2	0.25	$5\tau_{grid}$	
EXP3	0.25	$10\tau_{grid}$	
EXP4	0.50	$2\tau_{grid}$	
EXP5	0.50	$5\tau_{grid}$	$\mu = 0.1$
EXP6	0.50	$5\tau_{grid}$	$\mu = 0.05$
EXP7	0.50	$5\tau_{grid}$	$\mu = 0.01$
EXP8	0.50	$5\tau_{grid}$	$\tau_{01} = 1\tau_{grid}, \tau_{02} = 3\tau_{grid}$

List of Figures

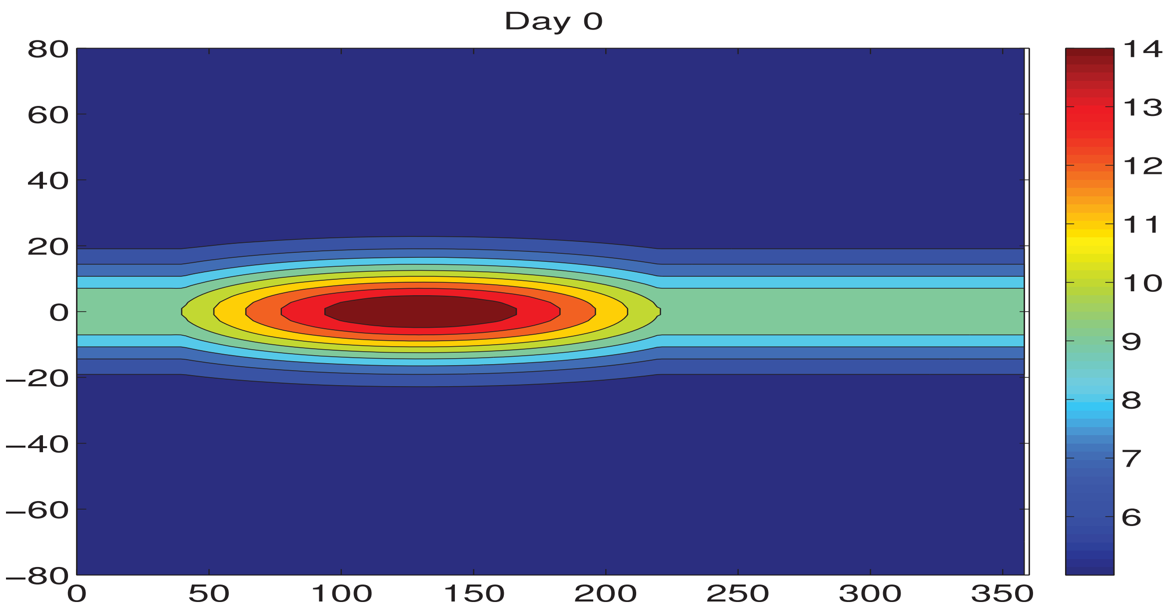

FIG. 1. Warm pool structure.

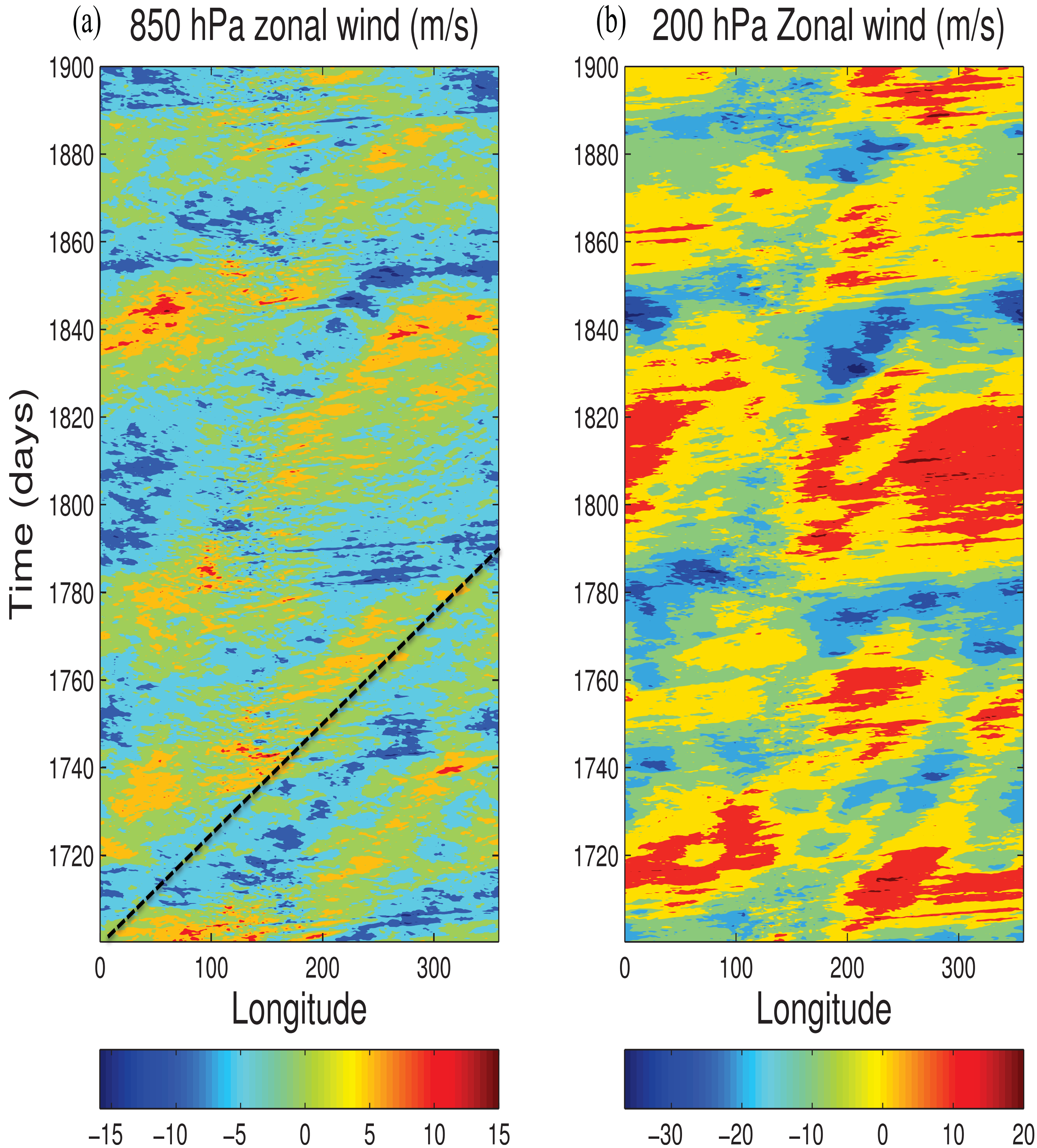

FIG. 2. Hovmöller diagram of meridionally averaged (10^oS-10^oN) zonal wind at (a) 850hPa and (b) 200 hPa in the standard parameter regime with $\alpha_s = 0.50$ and $\tau_{30} = 5\tau_{grid}$ (EXP1). The black dashed line marks an MJO-like event moving eastward at roughly 5 m s^{-1}.

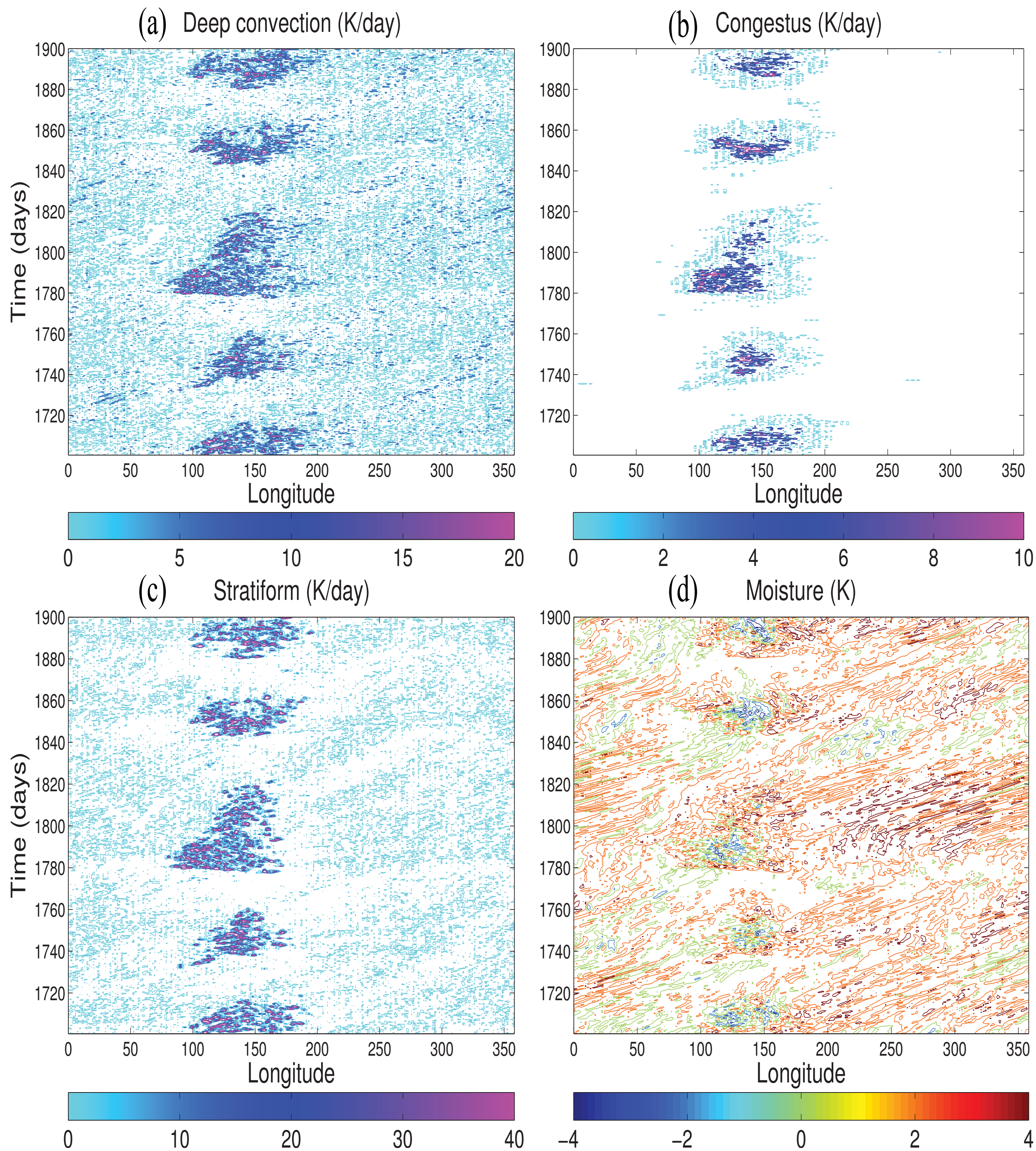

FIG. 3. Same as Figure 2 but for (a) deep convective, (b) congestus, and (c) stratiform heating rates and (d) vertically averaged moisture anomaly.

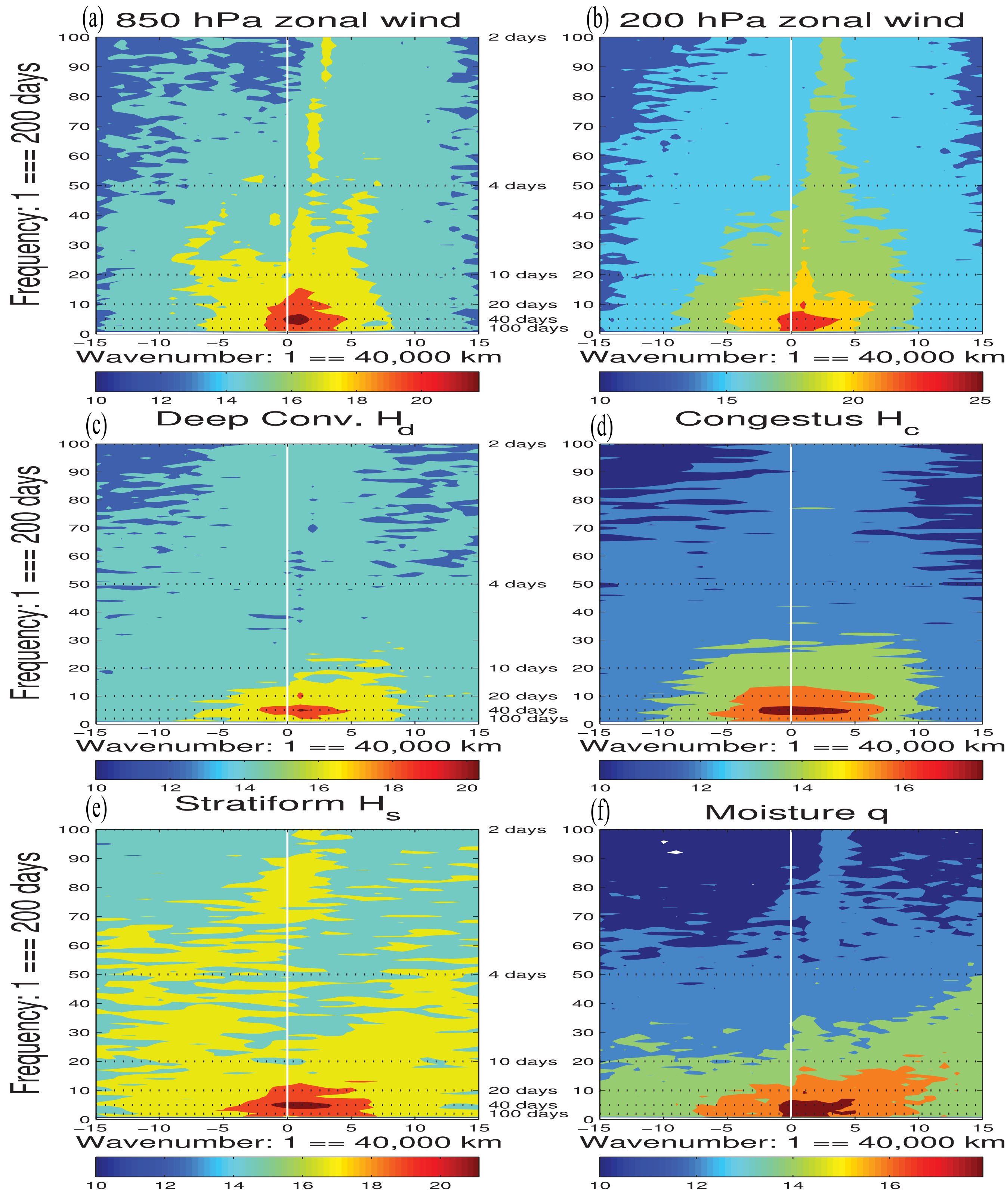

FIG. 4. Spectral power of the meridionally averaged (a) 800 hPa and (b) 200 hPa zonal wind, (c, d, e) convective heating rates and (f) moisture anomalies corresponding in Figure 2 and 3.

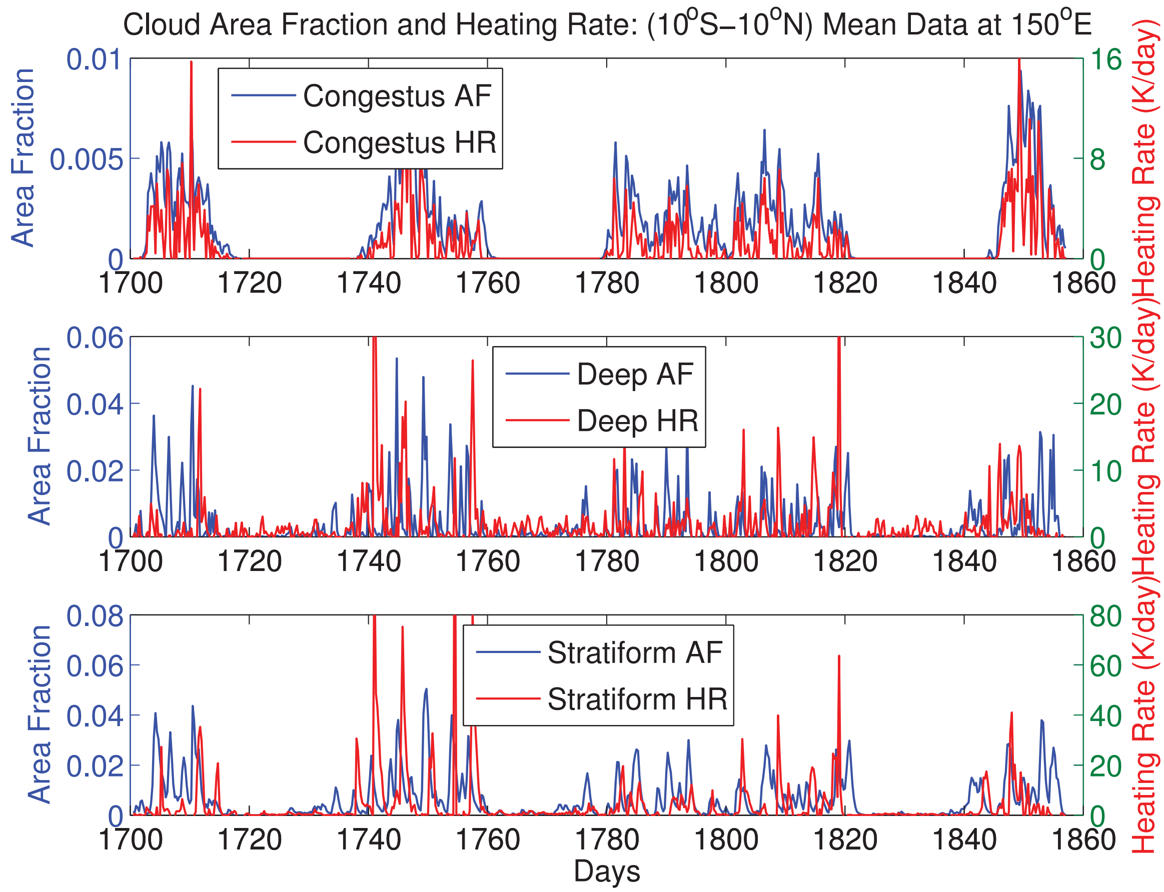

Fig. 5. Time series of the cloud area fractions (blue) and heating rates (red) averaged between 10^{o}S and 10^{o}N at 150^o longitude for EXP1.

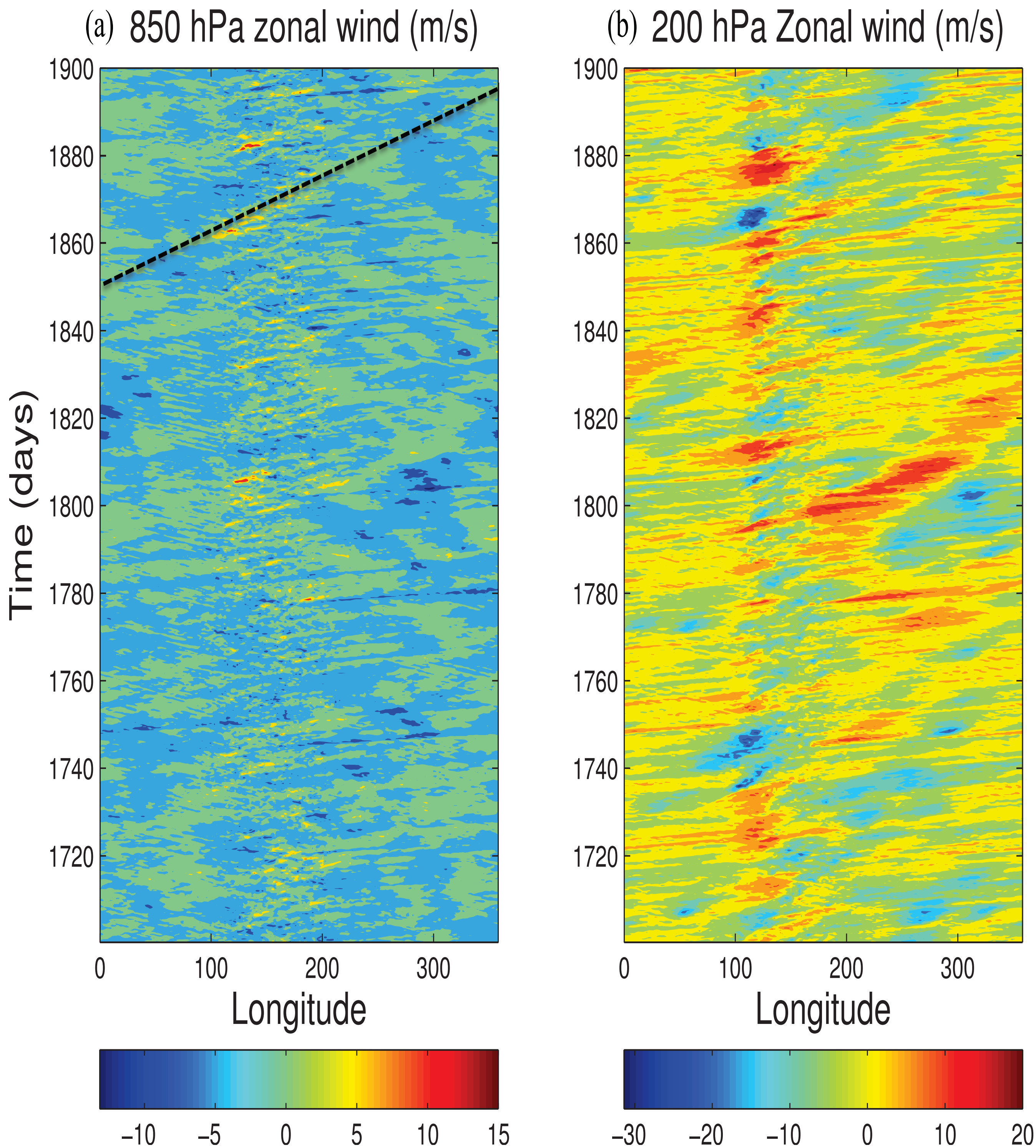

FIG. 6. Same as Figure 2 but with $\alpha_s = 0.25$ and $\tau_{30} = 5\tau_{grid}$ (EXP2). The black dashed line marks an eastward wavespeed about 10.3 m s^{-1}.

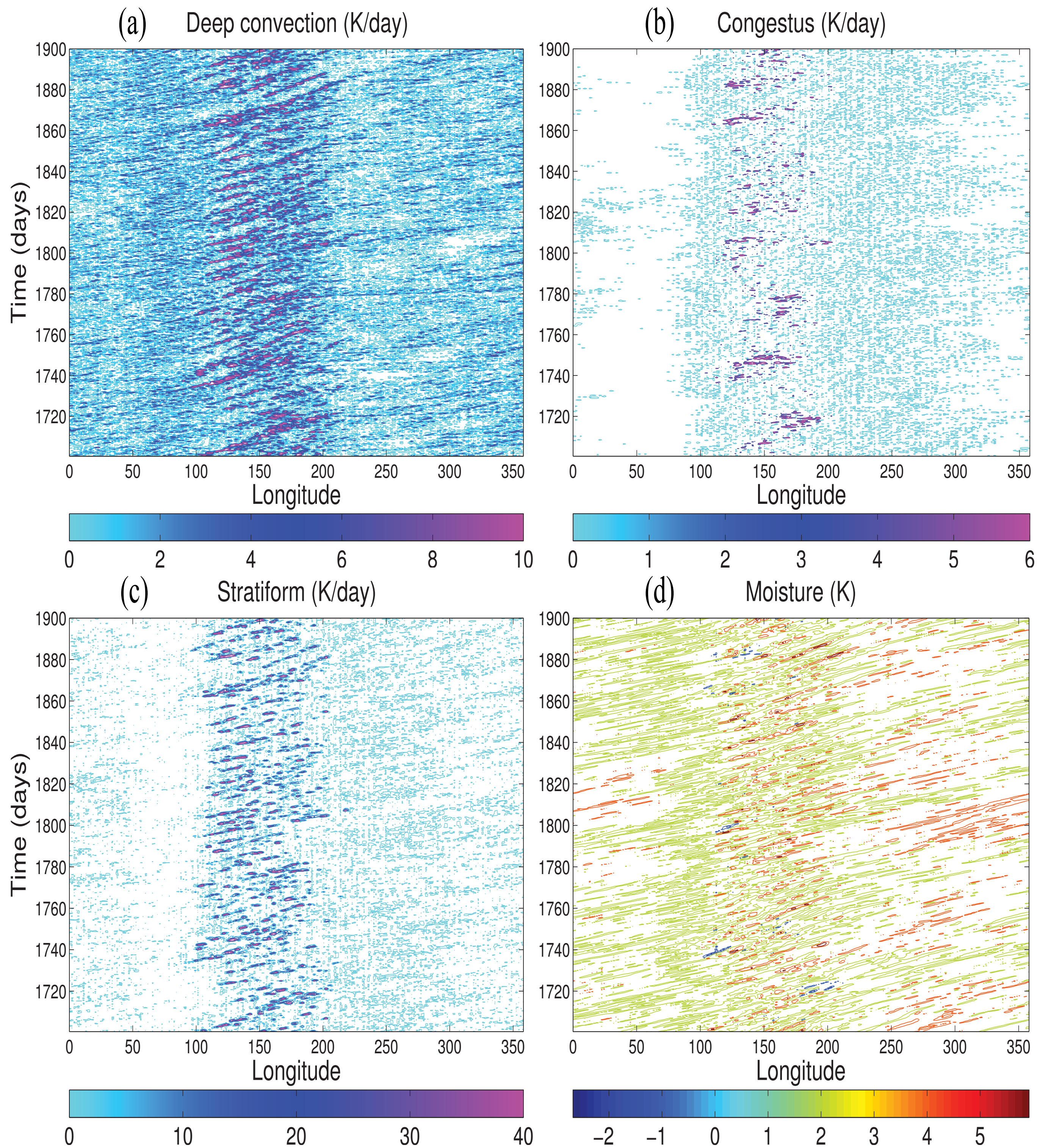

FIG. 7. Same as Figure 6 but for (a) deep, (b) congestus, and (c) stratiform heating rates and (d) moisture.

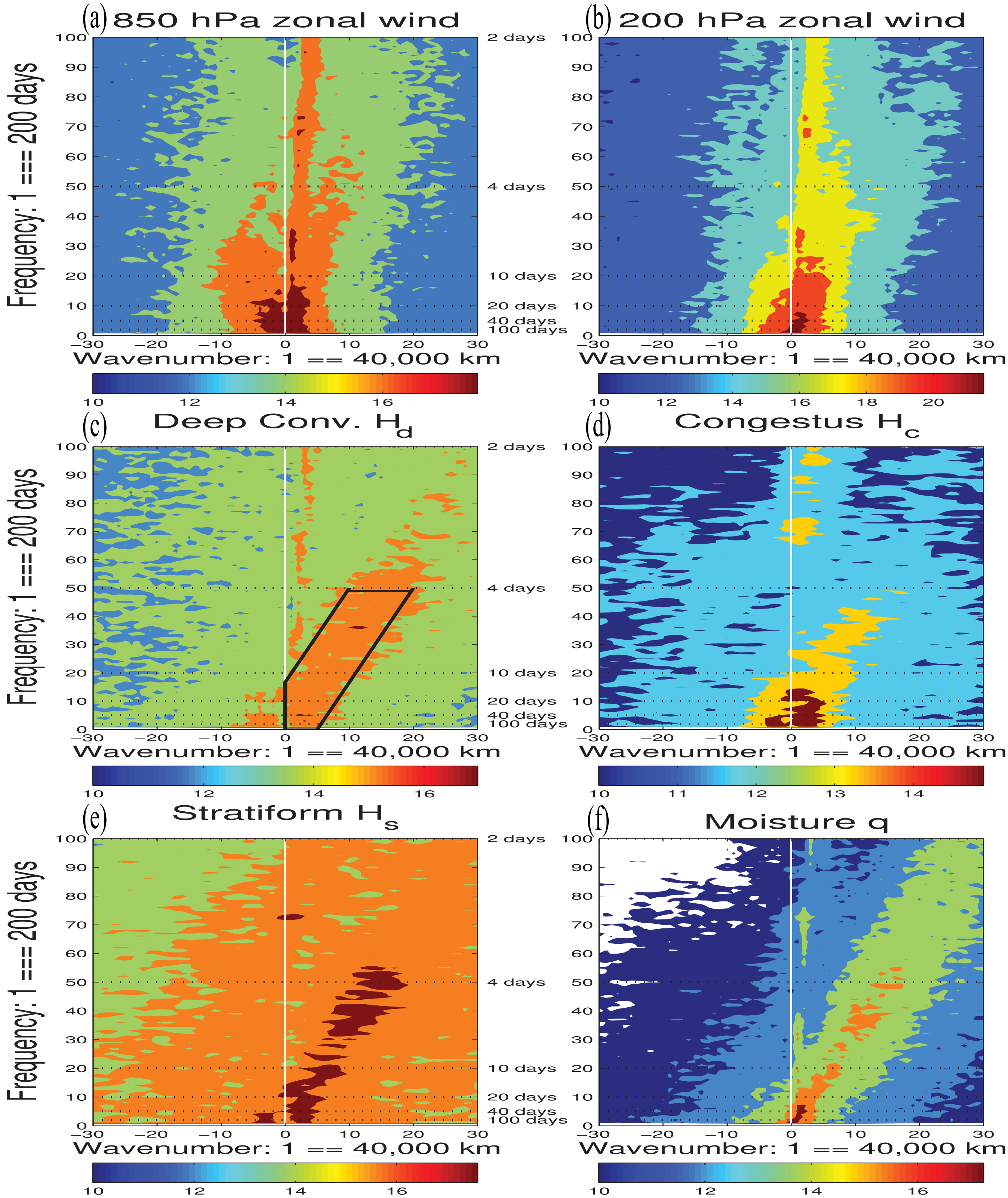

FIG. 8. Same as Figure 4 but for EXP2.

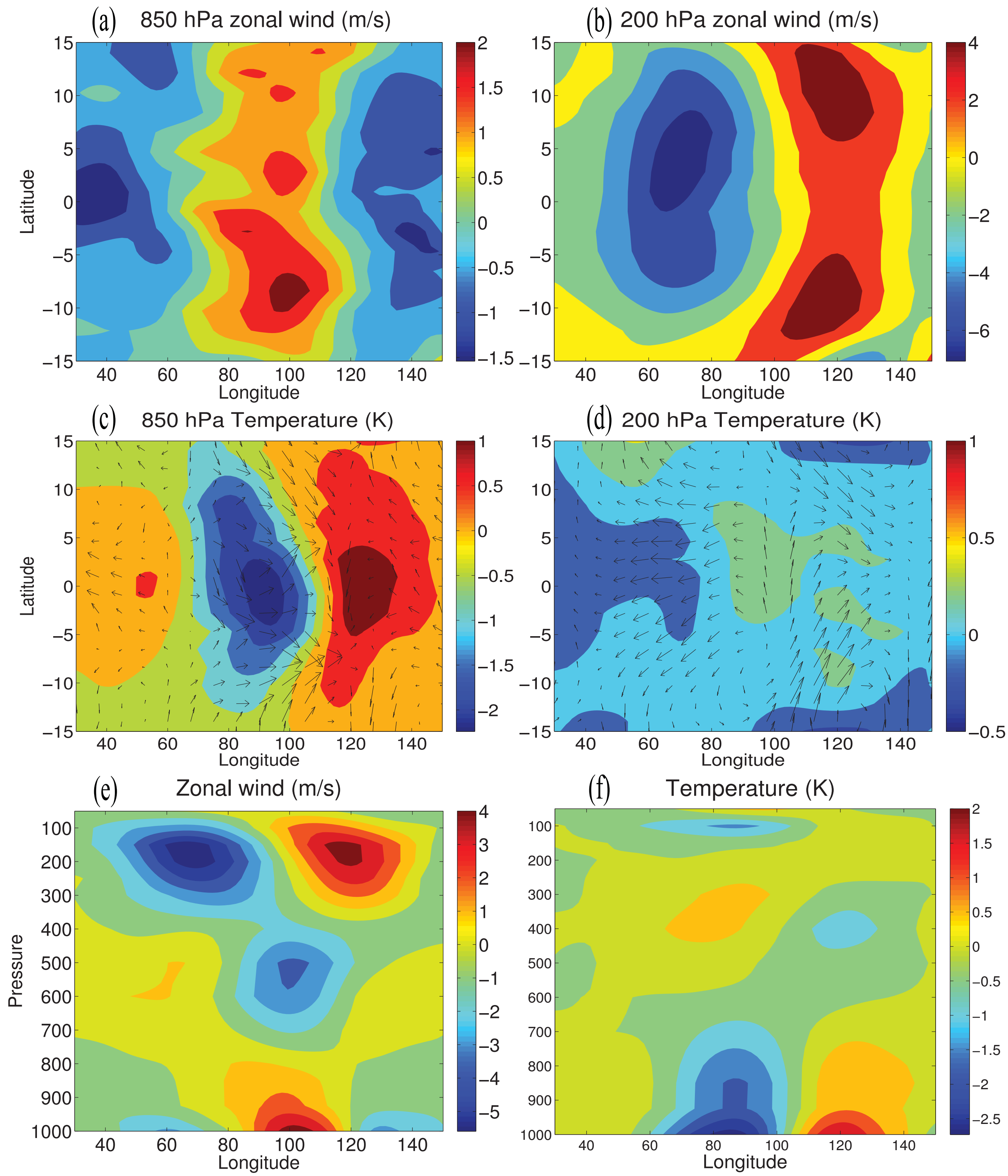

FIG. 9. Horizontal (a, b, c, d) and vertical (e, f) structures of convectively coupled waves from EXP2. The composite is obtained by first filtering in Fourier space using the window highlighted in Figure 8 and averaging the filtered data in time between day 1860 and day 1870 in the frame moving at 10.3 m s^{-1}.

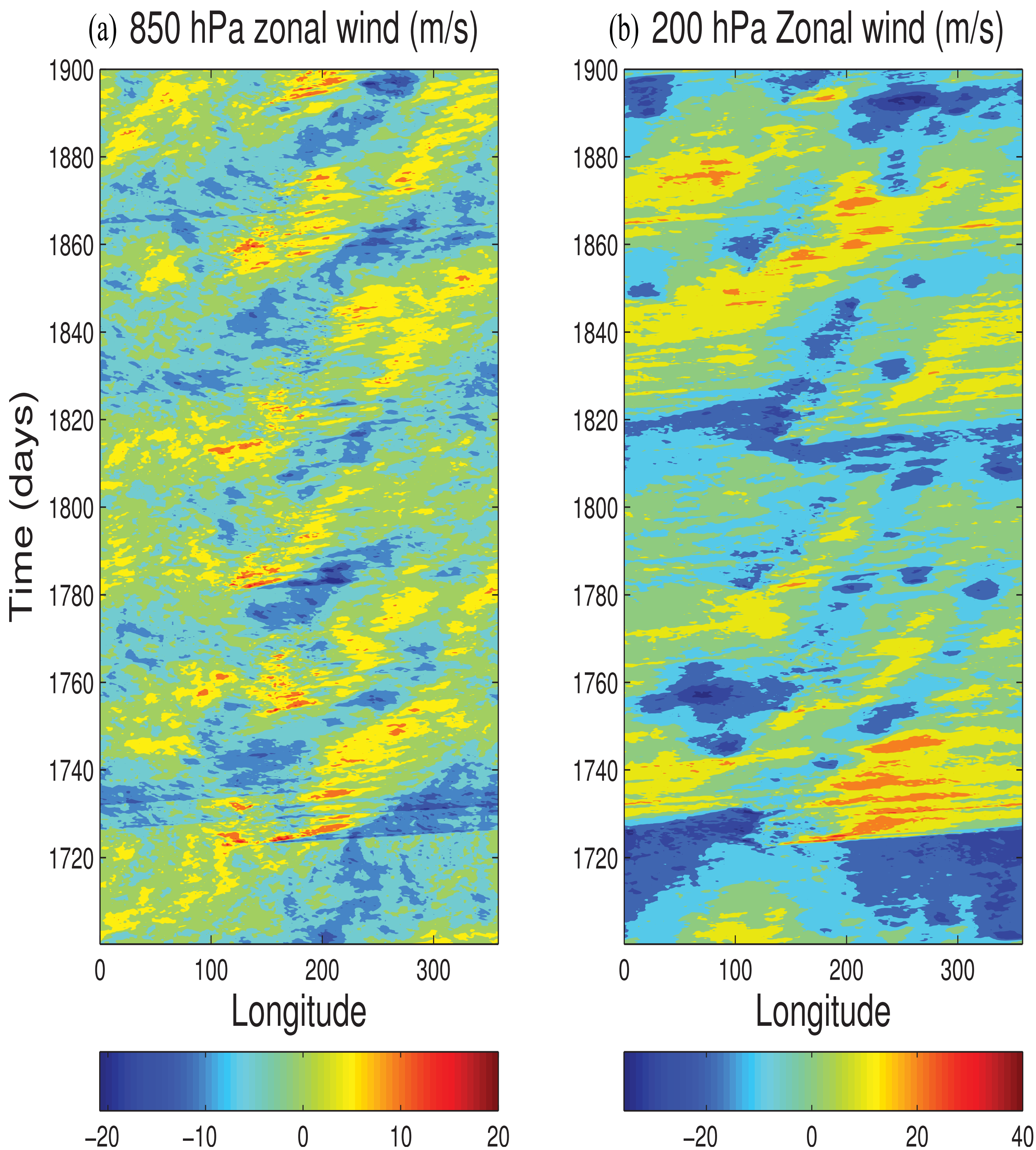

FIG. 10. Same as Figure 2 but with $\alpha_s = 0.25$ and $\tau_{30} = 10\tau_{grid}$ (EXP3).

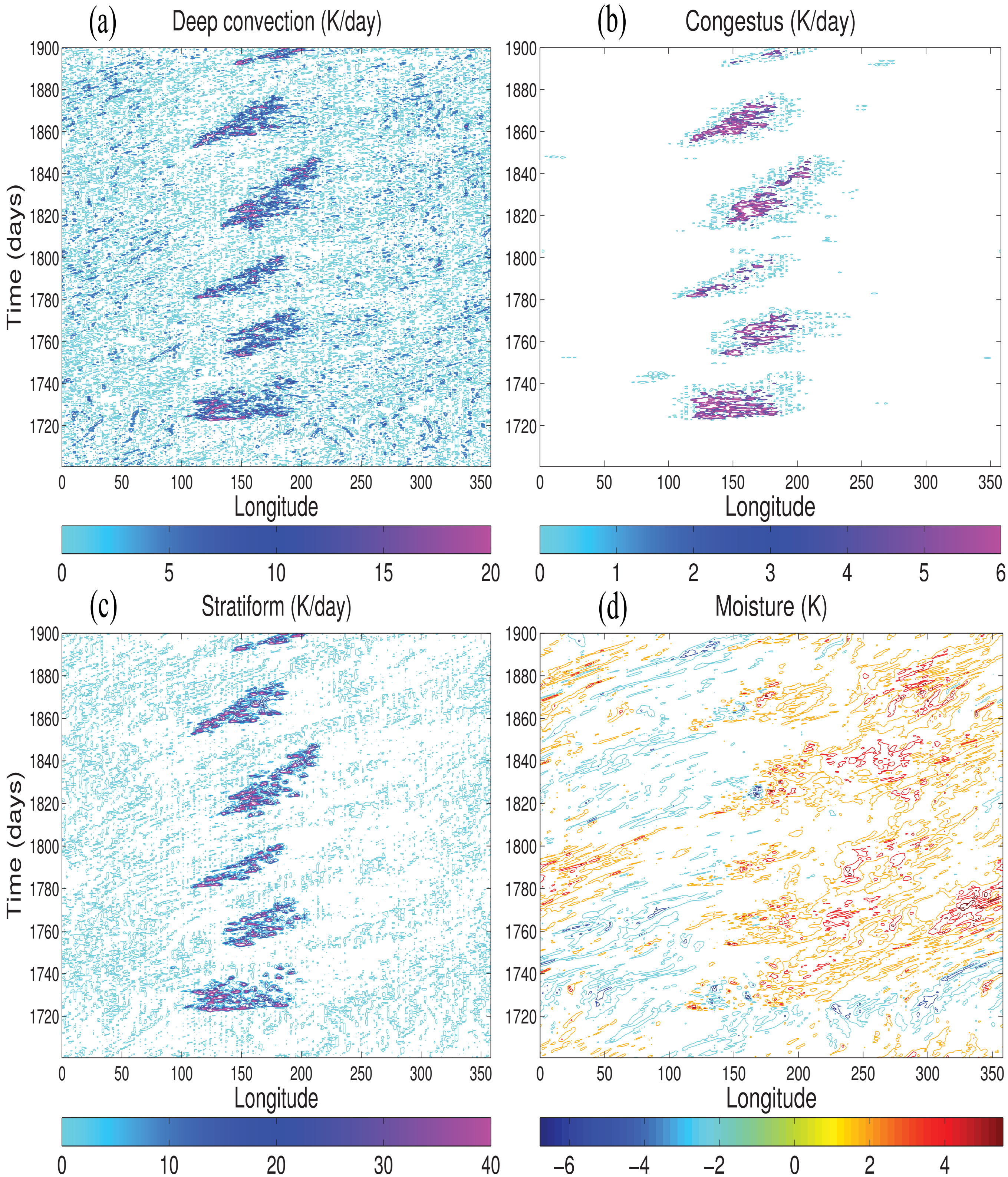

FIG. 11. Same as Figure 3 but with $\alpha_s = 0.25$ and $\tau_{30} = 10\tau_{grid}$ (EXP3).

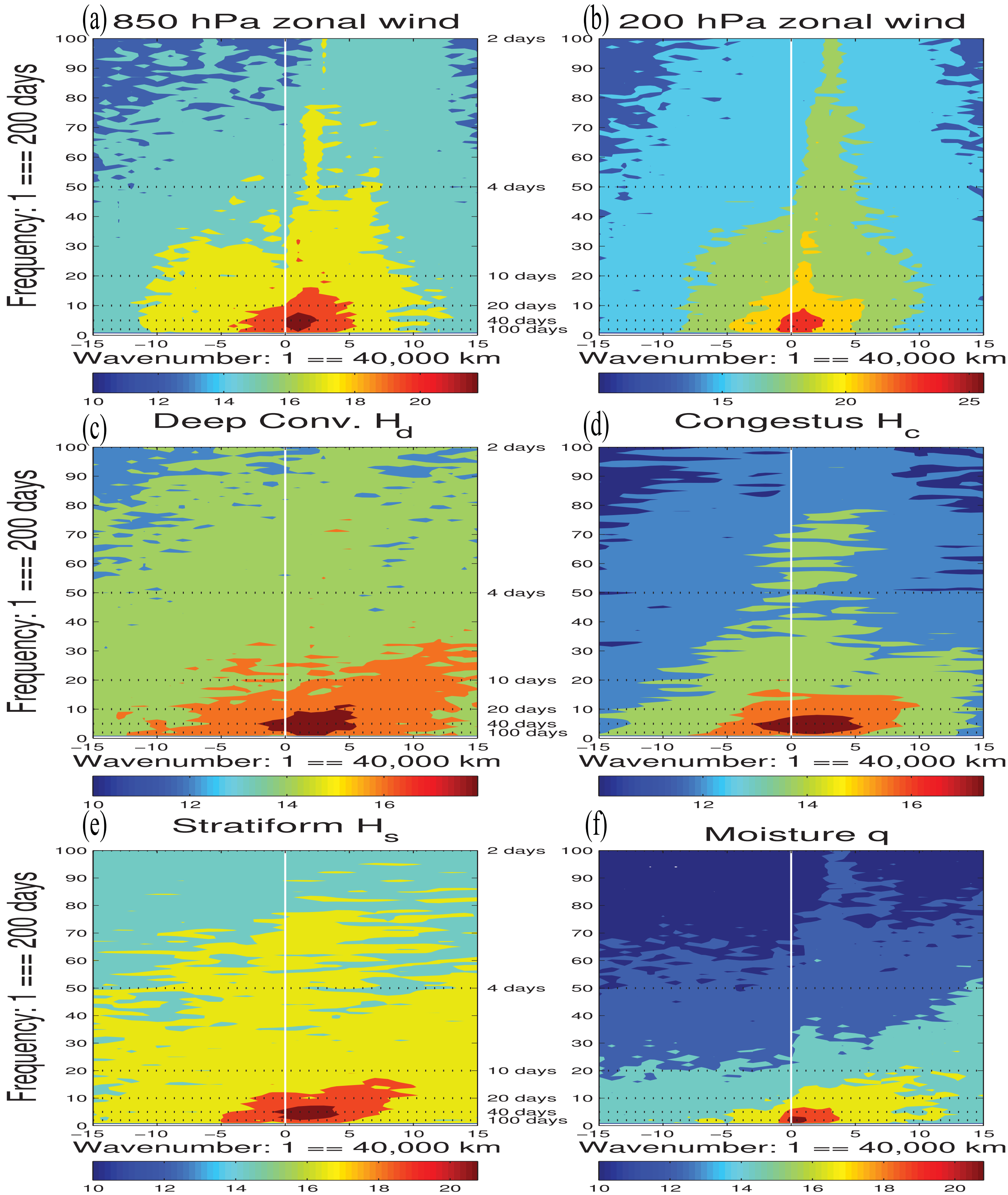

FIG. 12. Spectral power diagrams for EXP3: $\alpha_s = 0.25$ and $\tau_{30} = 10\tau_{grid}$.

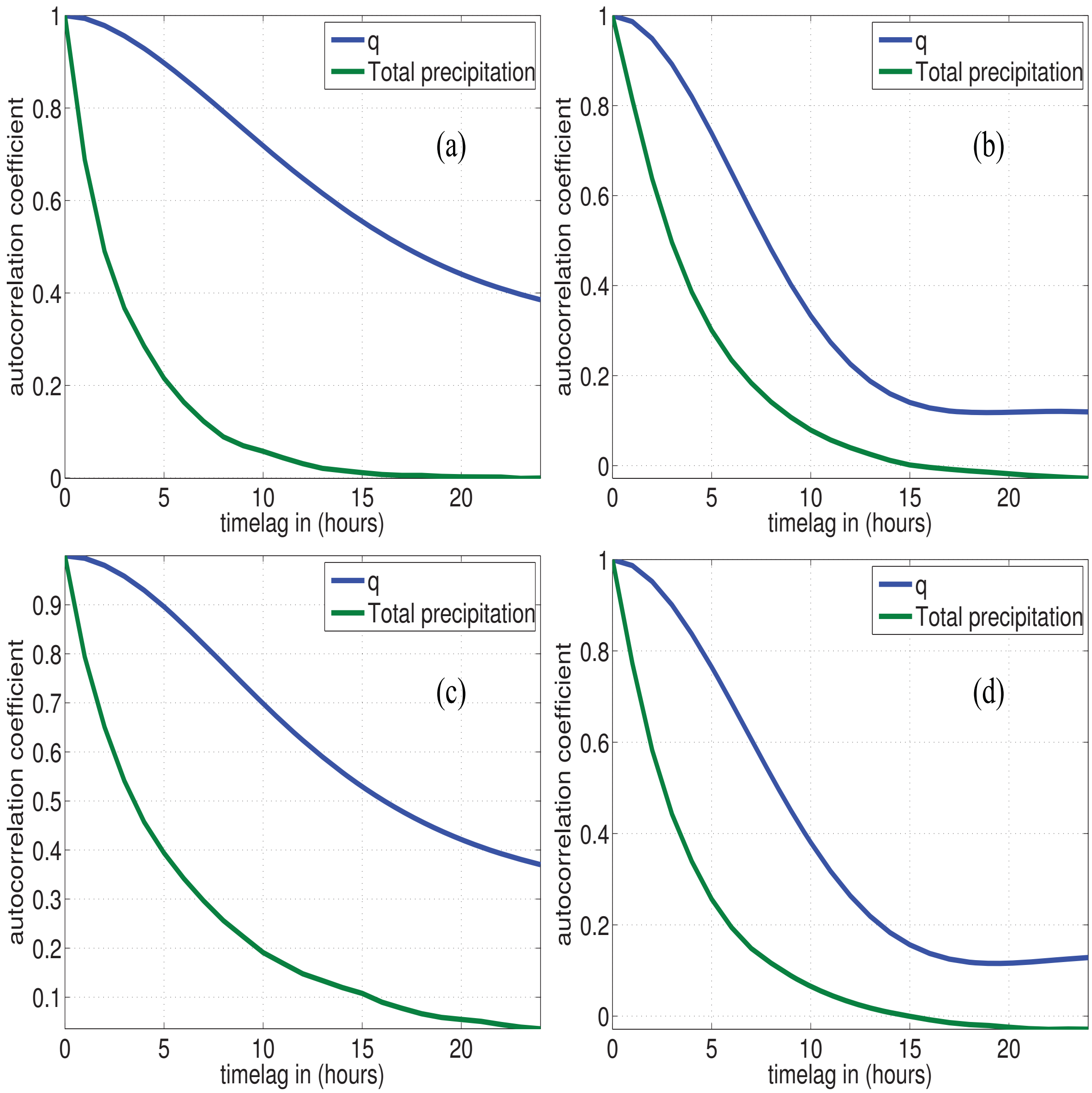

Fig. 13. Time auto-correlation functions of moisture (blue) and precipitation (green) for (a) EXP1, (b) EXP2, (c) EXP3 and (d) EXP4.

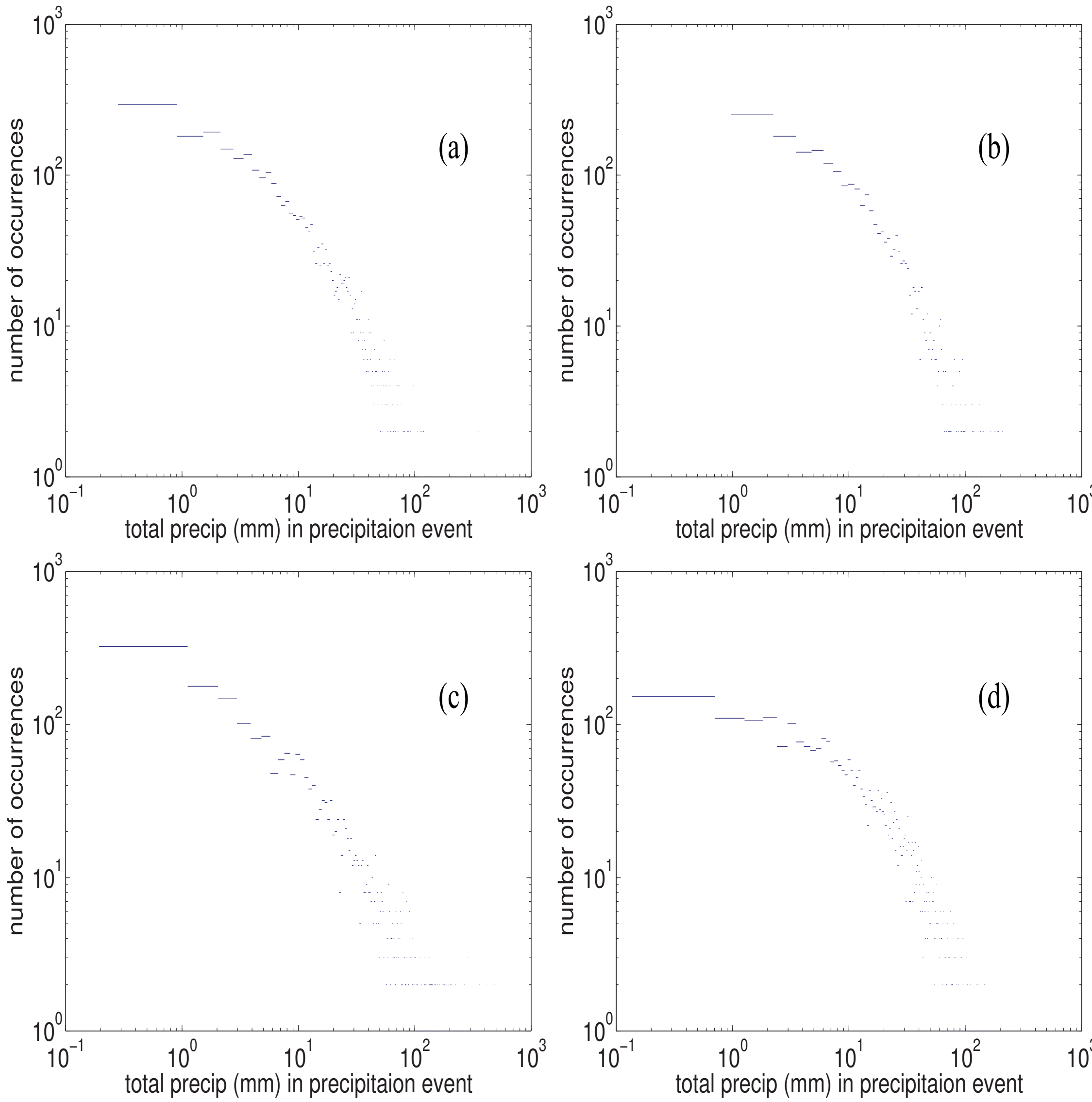

FIG. 14. Same as Figure 13 but for distribution of precipitation events.

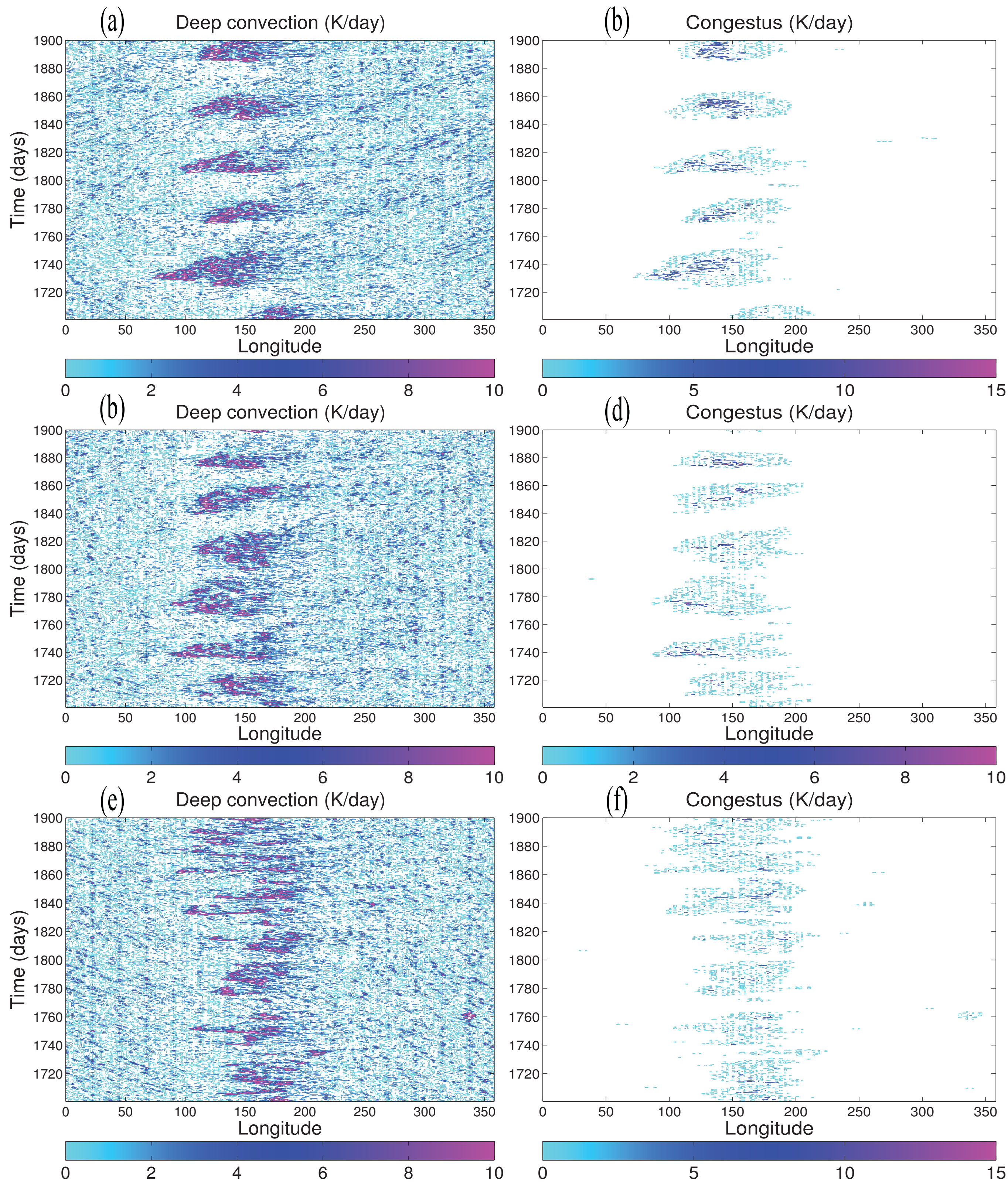

FIG. 15. Hovmoöller diagrams of deep convective (left) and congestus (right) heating rates for EXP5 (a,b), 6 (c,d) and 7 (e,f): $\alpha_s = 0.50$, $\tau_{30} = 5\tau_{grid}$ and $\mu = 0.1, 0.05, 0.01$ for respectively.

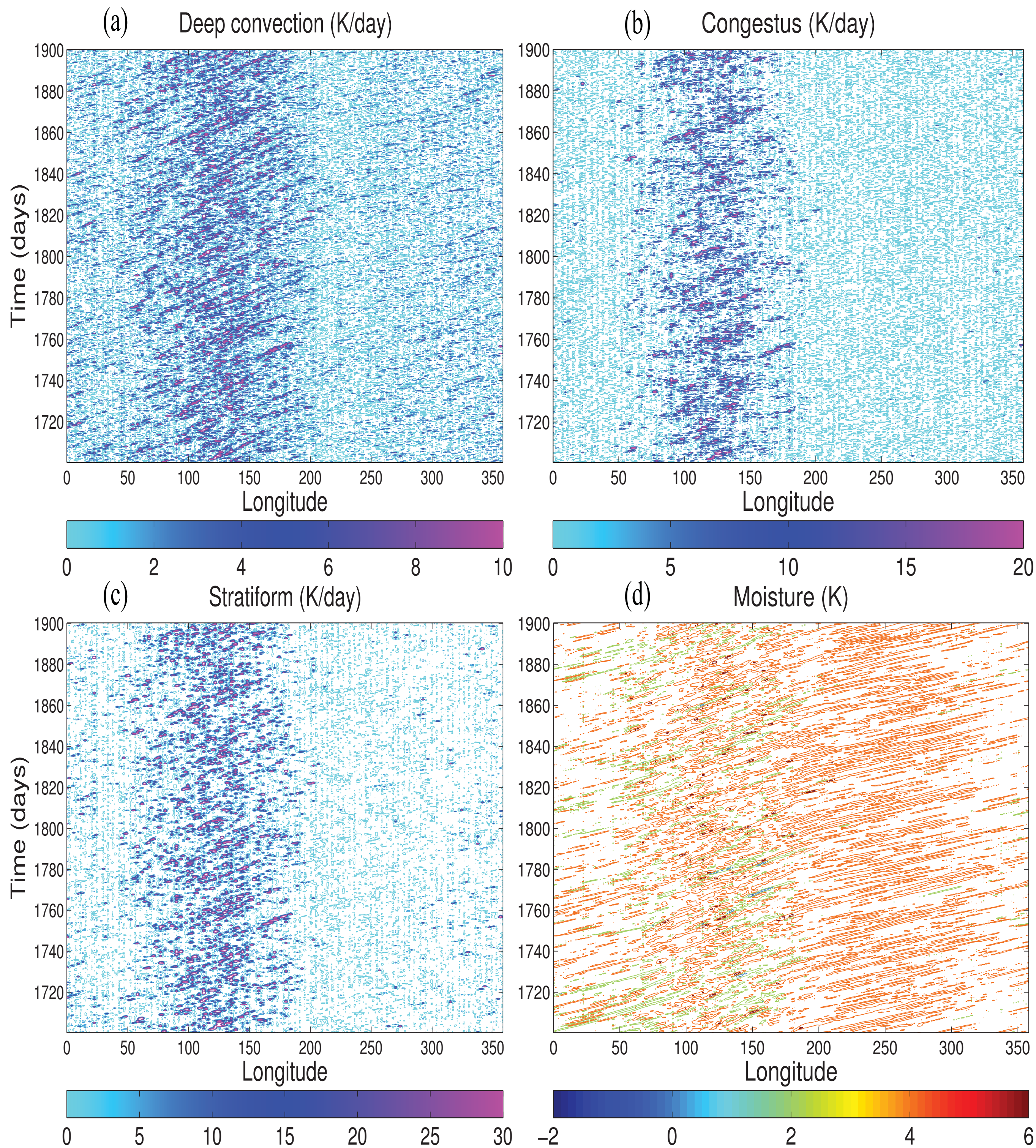

Fig. 16. Hovmöller diagram of (a, b, c) heating rates and (d) moisture for the case with DKM15 parameters: $\alpha_s = 0.50$, $\tau_{30} = 5\tau_{grid}$, $\tau_{01} = 1\tau_{grid}$ and $\tau_{02} = 3\tau_{grid}$ (EXP8).